EUROPEAN ORGANIZATION FOR NUCLEAR RESEARCH (CERN)

CERN-PH-EP/2006-011
May 11, 2006

Search for Higgs bosons decaying to WW in e^+e^- collisions at LEP

The ALEPH Collaboration *)

Abstract

A search for Higgs bosons produced in association with a fermion pair, and decaying to WW, is performed with the data collected by the ALEPH detector at centre-of-mass energies ranging from 191 to 209 GeV. The data correspond to an integrated luminosity of 453.2 pb^{-1}. Thirteen exclusive selections are developed according to the different final state topologies. No statistically significant evidence for a Higgs boson decaying into a WW pair has been found. An upper limit is derived, as a function of the Higgs boson mass, on the product of the $e^+e^- \to Hf\bar{f}$ cross section and the $H \to WW$ branching ratio. The data on the search for $H \to WW$ are combined with previously published ALEPH results on the search for $H \to \gamma\gamma$, to significantly extend the limits on the mass of a fermiophobic Higgs boson.

Submitted to Eur. Phys. J.C

*)See next pages for the list of authors

The ALEPH Collaboration

S. Schael,

Physikalisches Institut das RWTH-Aachen, D-52056 Aachen, Germany

R. Barate, R. Brunelière, I. De Bonis, D. Decamp, C. Goy, S. Jézéquel, J.-P. Lees, F. Martin, E. Merle, M.-N. Minard, B. Pietrzyk, B. Trocmé

Laboratoire de Physique des Particules (LAPP), IN^{2}P^3-CNRS, F-74019 Annecy-le-Vieux Cedex, France

S. Bravo, M.P. Casado, M. Chmeissani, J.M. Crespo, E. Fernandez, M. Fernandez-Bosman, Ll. Garrido,[15] M. Martinez, A. Pacheco, H. Ruiz

Institut de Física d'Altes Energies, Universitat Autònoma de Barcelona, E-08193 Bellaterra (Barcelona), Spain[7]

A. Colaleo, D. Creanza, N. De Filippis, M. de Palma, G. Iaselli, G. Maggi, M. Maggi, S. Nuzzo, A. Ranieri, G. Raso,[24] F. Ruggieri, G. Selvaggi, L. Silvestris, P. Tempesta, A. Tricomi,[3] G. Zito

Dipartimento di Fisica, INFN Sezione di Bari, I-70126 Bari, Italy

X. Huang, J. Lin, Q. Ouyang, T. Wang, Y. Xie, R. Xu, S. Xue, J. Zhang, L. Zhang, W. Zhao

Institute of High Energy Physics, Academia Sinica, Beijing, The People's Republic of China[8]

D. Abbaneo, T. Barklow,[26] O. Buchmüller,[26] M. Cattaneo, B. Clerbaux,[23] H. Drevermann, R.W. Forty, M. Frank, F. Gianotti, J.B. Hansen, J. Harvey, D.E. Hutchcroft,[30], P. Janot, B. Jost, M. Kado,[2] P. Mato, A. Moutoussi, F. Ranjard, L. Rolandi, D. Schlatter, F. Teubert, A. Valassi, I. Videau

European Laboratory for Particle Physics (CERN), CH-1211 Geneva 23, Switzerland

F. Badaud, S. Dessagne, A. Falvard,[20] D. Fayolle, P. Gay, J. Jousset, B. Michel, S. Monteil, D. Pallin, J.M. Pascolo, P. Perret

Laboratoire de Physique Corpusculaire, Université Blaise Pascal, IN^{2}P^3-CNRS, Clermont-Ferrand, F-63177 Aubière, France

J.D. Hansen, J.R. Hansen, P.H. Hansen, A.C. Kraan, B.S. Nilsson

Niels Bohr Institute, 2100 Copenhagen, DK-Denmark[9]

A. Kyriakis, C. Markou, E. Simopoulou, A. Vayaki, K. Zachariadou

Nuclear Research Center Demokritos (NRCD), GR-15310 Attiki, Greece

A. Blondel,[12] J.-C. Brient, F. Machefert, A. Rougé, H. Videau

Laoratoire Leprince-Ringuet, Ecole Polytechnique, IN^{2}P^3-CNRS, F-91128 Palaiseau Cedex, France

V. Ciulli, E. Focardi, G. Parrini

Dipartimento di Fisica, Università di Firenze, INFN Sezione di Firenze, I-50125 Firenze, Italy

A. Antonelli, M. Antonelli, G. Bencivenni, F. Bossi, G. Capon, F. Cerutti, V. Chiarella, P. Laurelli, G. Mannocchi,[5] G.P. Murtas, L. Passalacqua

Laboratori Nazionali dell'INFN (LNF-INFN), I-00044 Frascati, Italy

J. Kennedy, J.G. Lynch, P. Negus, V. O'Shea, A.S. Thompson

Department of Physics and Astronomy, University of Glasgow, Glasgow G12 8QQ,United Kingdom[10]

S. Wasserbaech

Utah Valley State College, Orem, UT 84058, U.S.A.

R. Cavanaugh,[4] S. Dhamotharan,[21] C. Geweniger, P. Hanke, V. Hepp, E.E. Kluge, A. Putzer, H. Stenzel,

K. Tittel, M. Wunsch[19]

Kirchhoff-Institut für Physik, Universität Heidelberg, D-69120 Heidelberg, Germany[16]

R. Beuselinck, W. Cameron, G. Davies, P.J. Dornan, M. Girone,[1] N. Marinelli, J. Nowell, S.A. Rutherford, J.K. Sedgbeer, J.C. Thompson,[14] R. White

Department of Physics, Imperial College, London SW7 2BZ, United Kingdom[10]

V.M. Ghete, P. Girtler, E. Kneringer, D. Kuhn, G. Rudolph

Institut für Experimentalphysik, Universität Innsbruck, A-6020 Innsbruck, Austria[18]

E. Bouhova-Thacker, C.K. Bowdery, D.P. Clarke, G. Ellis, A.J. Finch, F. Foster, G. Hughes, R.W.L. Jones, M.R. Pearson, N.A. Robertson, M. Smizanska

Department of Physics, University of Lancaster, Lancaster LA1 4YB, United Kingdom[10]

O. van der Aa, C. Delaere,[28] G.Leibenguth,[31] V. Lemaitre[29]

Institut de Physique Nucléaire, Département de Physique, Université Catholique de Louvain, 1348 Louvain-la-Neuve, Belgium

U. Blumenschein, F. Hölldorfer, K. Jakobs, F. Kayser, A.-S. Müller, B. Renk, H.-G. Sander, S. Schmeling, H. Wachsmuth, C. Zeitnitz, T. Ziegler

Institut für Physik, Universität Mainz, D-55099 Mainz, Germany[16]

A. Bonissent, P. Coyle, C. Curtil, A. Ealet, D. Fouchez, P. Payre, A. Tilquin

Centre de Physique des Particules de Marseille, Univ Méditerranée, IN^{2}P^3-CNRS, F-13288 Marseille, France

F. Ragusa

Dipartimento di Fisica, Università di Milano e INFN Sezione di Milano, I-20133 Milano, Italy.

A. David, H. Dietl,[32] G. Ganis,[27] K. Hüttmann, G. Lütjens, W. Männer[32], H.-G. Moser, R. Settles, M. Villegas, G. Wolf

Max-Planck-Institut für Physik, Werner-Heisenberg-Institut, D-80805 München, Germany[16]

J. Boucrot, O. Callot, M. Davier, L. Duflot, J.-F. Grivaz, Ph. Heusse, A. Jacholkowska,[6] L. Serin, J.-J. Veillet

Laboratoire de l'Accélérateur Linéaire, Université de Paris-Sud, IN^{2}P^3-CNRS, F-91898 Orsay Cedex, France

P. Azzurri, G. Bagliesi, T. Boccali, L. Foà, A. Giammanco, A. Giassi, F. Ligabue, A. Messineo, F. Palla, G. Sanguinetti, A. Sciabà, G. Sguazzoni, P. Spagnolo, R. Tenchini, A. Venturi, P.G. Verdini

Dipartimento di Fisica dell'Università, INFN Sezione di Pisa, e Scuola Normale Superiore, I-56010 Pisa, Italy

O. Awunor, G.A. Blair, G. Cowan, A. Garcia-Bellido, M.G. Green, T. Medcalf,[25] A. Misiejuk, J.A. Strong, P. Teixeira-Dias

Department of Physics, Royal Holloway & Bedford New College, University of London, Egham, Surrey TW20 OEX, United Kingdom[10]

R.W. Clifft, T.R. Edgecock, P.R. Norton, I.R. Tomalin, J.J. Ward

Particle Physics Dept., Rutherford Appleton Laboratory, Chilton, Didcot, Oxon OX11 OQX, United Kingdom[10]

B. Bloch-Devaux, D. Boumediene, P. Colas, B. Fabbro, E. Lançon, M.-C. Lemaire, E. Locci, P. Perez, J. Rander, B. Tuchming, B. Vallage

CEA, DAPNIA/Service de Physique des Particules, CE-Saclay, F-91191 Gif-sur-Yvette Cedex, France[17]

A.M. Litke, G. Taylor

Institute for Particle Physics, University of California at Santa Cruz, Santa Cruz, CA 95064, USA[22]

C.N. Booth, S. Cartwright, F. Combley,[25] P.N. Hodgson, M. Lehto, L.F. Thompson

Department of Physics, University of Sheffield, Sheffield S3 7RH, United Kingdom[10]

A. Böhrer, S. Brandt, C. Grupen, J. Hess, A. Ngac, G. Prange

Fachbereich Physik, Universität Siegen, D-57068 Siegen, Germany[16]

C. Borean, G. Giannini

Dipartimento di Fisica, Università di Trieste e INFN Sezione di Trieste, I-34127 Trieste, Italy

H. He, J. Putz, J. Rothberg

Experimental Elementary Particle Physics, University of Washington, Seattle, WA 98195 U.S.A.

S.R. Armstrong, K. Berkelman, K. Cranmer, D.P.S. Ferguson, Y. Gao,[13] S. González, O.J. Hayes, H. Hu, S. Jin, J. Kile, P.A. McNamara III, J. Nielsen, Y.B. Pan, J.H. von Wimmersperg-Toeller, W. Wiedenmann, J. Wu, Sau Lan Wu, X. Wu, G. Zobernig

Department of Physics, University of Wisconsin, Madison, WI 53706, USA[11]

G. Dissertori

Institute for Particle Physics, ETH Hönggerberg, 8093 Zürich, Switzerland.

[1]Also at CERN, 1211 Geneva 23, Switzerland.

[2]Now at Fermilab, PO Box 500, MS 352, Batavia, IL 60510, USA

[3]Also at Dipartimento di Fisica di Catania and INFN Sezione di Catania, 95129 Catania, Italy.

[4]Now at University of Florida, Department of Physics, Gainesville, Florida 32611-8440, USA

[5]Also IFSI sezione di Torino, INAF, Italy.

[6]Also at Groupe d'Astroparticules de Montpellier, Université de Montpellier II, 34095, Montpellier, France.

[7]Supported by CICYT, Spain.

[8]Supported by the National Science Foundation of China.

[9]Supported by the Danish Natural Science Research Council.

[10]Supported by the UK Particle Physics and Astronomy Research Council.

[11]Supported by the US Department of Energy, grant DE-FG0295-ER40896.

[12]Now at Departement de Physique Corpusculaire, Université de Genève, 1211 Genève 4, Switzerland.

[13]Also at Department of Physics, Tsinghua University, Beijing, The People's Republic of China.

[14]Supported by the Leverhulme Trust.

[15]Permanent address: Universitat de Barcelona, 08208 Barcelona, Spain.

[16]Supported by Bundesministerium für Bildung und Forschung, Germany.

[17]Supported by the Direction des Sciences de la Matière, C.E.A.

[18]Supported by the Austrian Ministry for Science and Transport.

[19]Now at SAP AG, 69185 Walldorf, Germany

[20]Now at Groupe d' Astroparticules de Montpellier, Université de Montpellier II, 34095 Montpellier, France.

[21]Now at BNP Paribas, 60325 Frankfurt am Mainz, Germany

[22]Supported by the US Department of Energy, grant DE-FG03-92ER40689.

[23]Now at Institut Inter-universitaire des hautes Energies (IIHE), CP 230, Université Libre de Bruxelles, 1050 Bruxelles, Belgique

[24]Now at Dipartimento di Fisica e Tecnologie Relative, Università di Palermo, Palermo, Italy.

[25]Deceased.

[26]Now at SLAC, Stanford, CA 94309, U.S.A

[27]Now at CERN, 1211 Geneva 23, Switzerland

[28]Research Fellow of the Belgium FNRS

[29]Research Associate of the Belgium FNRS

[30]Now at Liverpool University, Liverpool L69 7ZE, United Kingdom

[31]Supported by the Federal Office for Scientific, Technical and Cultural Affairs through the Interuniversity Attraction Pole P5/27

[32]Now at Henryk Niewodniczanski Institute of Nuclear Physics, Polish Academy of Sciences, Cracow, Poland

1 Introduction

A Higgs model [1] incorporating two doublets of complex scalar fields [2] generates five scalar Higgs bosons, three of which are neutral. In some types of models, for certain choices of parameters, one of these neutral scalars provides mass only to the fermions and another couples exclusively to the bosons, i.e. is a "fermiophobic" Higgs boson. Anomalous couplings in the Higgs sector can also enhance the bosonic branching fraction [3].

The search for a fermiophobic Higgs boson has been primarily carried out by the four LEP experiments in the $H \to \gamma\gamma$ channel, in which the Higgs boson couples to photons via a W loop [4, 5, 6, 7]. A benchmark fermiophobic Higgs boson is defined by considering Standard-Model-like couplings to bosons, and null couplings to fermions. Current analyses exclude the benchmark fermiophobic Higgs boson up to a mass of $109.7\,\mathrm{GeV}/c^2$ [8]. For fermiophobic Higgs bosons heavier than $90\,\mathrm{GeV}/c^2$, the predicted $H \to \gamma\gamma$ branching ratio becomes small relative to the predicted $H \to WW$ branching ratio (Fig. 1) motivating a search in this new channel. Such an analysis has already been carried out by the L3 collaboration [10] and is performed here with data collected by the ALEPH detector.

The main production processes at e^+e^- colliders for a fermiophobic Higgs boson are $e^+e^- \to Z^* \to ZH$ (Higgsstrahlung), WW and ZZ fusion. The cross sections of the boson fusion production processes are considerably smaller than that of the Higgsstrahlung process at LEP centre-of-mass (CM) energies. In the mass range kinematically accessible for Higgsstrahlung at LEP, one of the virtual W bosons is expected to be near on-shell, and the other (denoted W^*) to have a much smaller mass and energy. In this paper, all the signatures originating from the $Z \to q\bar{q}, \nu\bar{\nu}, \ell^+\ell^-$ decays and the $W, W^* \to q\bar{q}', \ell^\pm\nu$ decays are searched for. For simplicity and conciseness, the term "lepton" (and the corresponding symbol ℓ) refers to electrons and muons only. Leptonic tau decays are not specifically addressed, but the corresponding selected events are included in the final results. The hadronic tau decays in $e^+e^- \to ZWW^* \to \ell^+\ell^-\tau\nu q\bar{q}'$ are also looked for. The analysis is performed on the data taken in the years 1999 and 2000 at CM energies ranging from 191 to 209 GeV. The luminosities and CM energies are shown in Table 1.

This paper is organized as follows. A brief description of the ALEPH detector is given is Section 2. The signal and background simulations are summarized in Section 3. The overall search strategy is presented in Section 4 and the specific selection algorithms in Section 5. The results are reported in Section 6.

2 The ALEPH detector

A detailed description of the ALEPH detector can be found in Ref. [11], and of its performance in Ref. [12]. Here, only a brief description of the detector elements and the algorithms relevant to this analysis is given.

The trajectories of charged particles are measured with a silicon vertex detector (VDET), a cylindrical drift chamber (ITC) and a large time projection chamber (TPC), all immersed in a 1.5 T axial magnetic field provided by a superconducting solenoidal

coil. The energy of electrons, photons, and hadrons is measured with the electromagnetic (ECAL), the hadron (HCAL) and the luminosity (LCAL and SiCAL) calorimeters. The ECAL, placed between the TPC and the coil, is a highly segmented calorimeter, which is used to identify electrons and photons, and to measure their energy and position. The LCAL and SiCAL extend the calorimetric coverage down to 34 mrad from the beam axis. The HCAL consists of an instrumented iron return yoke. It provides the measurement of hadronic energy and, together with external chambers, muon identification.

In the following, *good* tracks (or simply tracks) are defined as charged particle tracks reconstructed with at least four hits in the time projection chamber, originating from within a cylinder of 20 cm length and 2 cm radius, coaxial with the beam and centred on the nominal collision point, and with a polar angle with respect to the beam such that $|\cos\theta| < 0.95$.

In this analysis, all searches make use of the same lepton identification criteria, where needed and applicable. Electrons are identified by comparing the momentum measured in the tracking detectors with the energy measured in the ECAL, by the depth and shape of the ECAL shower, and by the specific ionization information from the TPC, when available. Muons are identified by their characteristic hit pattern in the hadron calorimeter, and must have at least one associated hit in the muon chambers. Lepton identification is described in detail in Ref. [13].

Global event quantities, such as the total visible energy ($E_{\rm tot}$), the total visible mass ($M_{\rm tot}$), or the missing energy ($E_{\rm miss}$) are measured with an energy-flow algorithm [12], which combines individual tracker and calorimeter measurements into energy-flow "particles". These objects are classified as photons, electrons, muons, neutral or charged hadrons. The jets used in the present analysis are obtained by clustering the energy-flow particles with the Durham jet-finding algorithm [14], and allow various event topological variables to be determined. These include, for example, the acollinearity angle $\theta_{\rm aco}$(respectively the acoplanarity angle $\Phi_{\rm aco}$) between two jets (respectively between their projections onto the plane transverse to the beam axis) in an event forced to form two jets, the transition values y_{ij} of the resolution parameter $y_{\rm cut}$ at which the number of jets in an event switches from j to i jets, or the good track multiplicity $N_{{\rm ch},i}$ in jet i. Other specific variables, related either to the event topology, to the jet properties, or to the lepton characteristics, are described in turn in Section 5.

3 Simulated samples

Signal samples were generated using `HZHA` [9] for Higgs boson masses between 90 and 117 GeV/c^2 and at seven different CM energies: 191.6, 195.5, 199.5, 201.6, 204.9, 206.5 and 208 GeV, including Higgsstrahlung and fusion processes. All decays of the Z and W bosons were considered. In the `HZHA` code, there is no spin correlation between the W bosons coming from the Higgs boson decay. The signal events were therefore re-weighted to take into account this spin correlation. The event weight was computed as the ratio between the full four-fermion matrix element and the `HZHA` matrix element [15].

Event samples of all Standard Model (SM) background processes relevant for the Higgs boson search were also generated: the Bhabha process was simulated with `BHWIDE 1.01` [16], $q\bar{q}$, dimuon and ditau events with `KK 4.14` [17], $\gamma\gamma$ processes with `PHOT02` [18]. In the following, these processes will be grouped under the label "two-fermions". WW production was simulated with `KORALW 1.51` [19] and the remaining four-fermion processes with `PYTHIA 6.1` [20]. The background event samples were generated at the same CM energy values as the signal. The simulated sample sizes are at least a factor 20 greater than the data. A detailed simulation of the detector response was applied to both background and signal events.

4 Search strategy

4.1 Event classes, topological searches and targeted channels

The event selection is subdivided in a number of topological searches, each of which targets a specific final state (or channel) arising from the ZWW* production. The list of channels addressed in this paper is given in the second column of Table 2, with the Z, the W and the W* decays given in this order, together with the corresponding branching fractions. Altogether, almost 80% of the possible final states are targeted by the selection algorithms developed for this study.

Events are first separated in four exclusive classes according to the number and the energy of identified leptons in the final state. The four classes, further subdivided in different topologies (or subclasses), are defined as follows, and are displayed in the first column of Table 2.

- Fully Hadronic (Class 1): in this class, only events with neither energetic nor isolated identified leptons are selected. It addresses final states exclusively with hadronic jets, with (class 1a) or without (class 1b) missing energy, depending on whether the Z decays in a pair of quarks or a pair of neutrinos.
- Two Hard Leptons (Class 2): in this class, events with at least two energetic identified leptons are selected. It addresses final states in which the Z decays into a lepton pair. Five different topological searches were developed according to the W and W* decay modes.
- One Hard Lepton (class 3): in this class, events with exactly one energetic identified lepton are selected. It addresses final states in which the W decays to $\ell\nu$. Four different topologies were defined according to the hadronic activity and the missing energy, to target the remaining Z and W* decays.
- One Soft Lepton (class 4): in this class, events with exactly one isolated identified lepton that does not meet the momentum requirement of class 3 are selected, to address the W$^* \to \ell\nu$ decays. Two different topological searches were developed according to the hadronic activity and the missing energy, to address the hadronic and invisible Z decays.

These definitions, and the corresponding topological searches, were developed to minimize the cross-channel contamination between the different subclasses.

4.2 Topological search optimization

In each of the topological searches, the selection criteria were tailored to optimize the combined sensitivity to a Higgs boson mass hypothesis of $110\,\mathrm{GeV}/c^2$, which is near the expected experimental sensitivity in the fermiophobic scenario. To do so, the expected combined confidence level on the signal hypothesis, $\langle \mathrm{CL_s} \rangle$, that would be obtained on average if no signal were present, is minimized [21] with respect to the position of the cuts on most of the selection variables. An estimate of the value of $\langle \mathrm{CL_s} \rangle$ is determined with a toy Monte Carlo method using the approximate formula of Ref. [22], with the algorithm of Ref. [23].

For each topology, the determination of $\langle \mathrm{CL_s} \rangle$ requires the expected number of background events (N_b), the number of signal events expected from the targeted final state N_s, and the expected distribution of a variable D aimed at discriminating between the signal and the background. The observed values of the confidence levels on the signal and on the background hypotheses, $\mathrm{CL_s}$ and $\mathrm{CL_b}$, are obtained in the same way from the number of events observed (N_d) and the value of D for each of these events.

In the optimization process the values of N_b and N_s correspond to the CM energies and the integrated luminosity collected in the year 2000. Lower energy data sets would indeed not contribute significantly to the combined sensitivity to a $110\,\mathrm{GeV}/c^2$ Higgs boson signal, and are therefore absent from all distributions presented in Section 5. Since, however, they increase the sensitivity to smaller masses, the data taken in 1999 were included in the final result (Section 6).

5 Event selection

5.1 Preselection and class assignment

Common preselection cuts are applied in all four classes in order to strongly reduce the $\gamma\gamma$ and $\ell^+\ell^-$ backgrounds. The energy within 12° of the beam axis, E_{12}, must be less than 40% of the CM energy. The acollinearity must be less than 170° for events with less than four tracks. Finally, the total invariant mass M_tot and total transverse momentum P_t of the event must satisfy $M_\mathrm{tot} + 6P_t > 0.2\sqrt{s}$.

The event-to-(sub)class assignment is based on the energies E_{ℓ_i} and the isolations $I_{\ell_i} = 1 - \cos\theta_{\ell_i T}$ ($i = 1, 2, 3$) of the three most energetic leptons in the event. Here $\theta_{\ell_i T}$ is the angle between the ith lepton direction and the closest track in the event. If less than three leptons are found, the corresponding energies and isolation variables are set to 0 and 10^{-20} respectively. Events in which the most energetic lepton is "hard" ($E_{\ell_1} > 25\,\mathrm{GeV}$) are assigned to class 2 or 3 depending on the energy of the second most energetic lepton. To separate the remaining events between classes 1 and 4, a linear discriminant D_{14} is

built with E_{ℓ_1}, the total missing three-momentum (P_{miss}), and the isolation of the most energetic lepton (I_{ℓ_1}):

$$D_{14} = 2.3E_{\ell_1} + P_{\text{miss}} + 4.8\ln(I_{\ell_1}). \quad (1)$$

Details of the partition process are presented in Table 3. The criteria used to define all the subclasses presented in Section 4.1 are also shown in the table. Subclasses 1a and 1b are separated by a cut on the missing mass M_{miss}. Subclasses 2a and 2t are separated from subclasses 2b, 2c and 2d with a cut on E_{ℓ_3}. Subclass 2b is finally identified with a cut on the total hadronic energy, E_{had}. Subclasses 2c and 2d are separated from each other by a cut on the number of tracks (N_{ch}) while subclasses 2a and 2t are distinguished using the hadronic activity. The separation between subclasses 3a, 3b and 3c, 3d is achieved by cutting on the total and missing invariant mass of the event. A cut on the energy of the second most energetic lepton is used to distinguish subclasses 3a, 3d from 3b, 3c. Finally, subclasses 4a and 4b are separated from each other by cutting on the total invariant mass of the event.

5.2 Class 1: Fully hadronic final state

5.2.1 Class 1a: Six-jets final state

targeted channel: $\text{ZH} \to \text{q}\bar{\text{q}}\,\text{q}\bar{\text{q}}\,\text{q}\bar{\text{q}}$

This subclass is characterized by a final state with a large number of tracks, a value of the total mass divided by the CM energy ($M_{\text{tot}}/\sqrt{s}$) close to 1, no missing longitudinal momentum ($P_l/\sqrt{s}$), an intermediate sphericity (S) [24], and a high value of $\ln(y_{34})$. Corresponding preselection cuts are applied, in addition to those applied in the four classes, and are presented in Table 4, together with the numbers of selected data, background and signal events. After the preselection, the background is dominated by WW events.

The final selection cuts are given in the lower section of Table 4. The variables $N^{\text{min}}_{\text{ch,j6}}$, $\theta^{\text{min}}_{\text{j6}}$ and $\theta^{\text{max}}_{\text{j6}}$ are computed after having forced the event to be clustered into six jets. The smallest number of tracks in any jet is denoted $N^{\text{min}}_{\text{ch,j6}}$, and the variables $\theta^{\text{min}}_{\text{j6}}$ and $\theta^{\text{max}}_{\text{j6}}$ represent the smallest and largest angle between any pair of jets. The jet pair with the invariant mass closest to $91.2\,\text{GeV}/c^2$ is assigned to the Z. The two least energetic jets are assigned to the W^*, and the remaining two jets to the W. The invariant mass of the Z, W and W^* are denoted M_1, M_2 and M_3, respectively.

The discriminant variable M_2 enters the CL_s computation and is shown in Figs. 2a and 2b, after the preselection and the final selection, respectively. In this subclass, the targeted-signal efficiency is 61% and the number of expected background events is 163.7.

5.2.2 Class 1b: Four-jets and missing transverse momentum final state

targeted channel: $\text{ZH} \to \nu\bar{\nu}\,\text{q}\bar{\text{q}}\,\text{q}\bar{\text{q}}$

This subclass is characterized by a final state with a large missing mass. The preselection cuts used for subclass 1a are also relevant with, in general, weaker cut values, as shown

in Table 5. The class 1b preselection has two additional cuts on the value of the cosine of the polar angle of the missing momentum $\cos(\theta_{\text{miss}})$ and on E_{12}. After the preselection, the proportion of main background events is 43% WW, 30% $\mathrm{q\bar{q}}$, 12% Weν and 12% ZZ.

The final selection cuts are detailed in the lower section of Table 5. The acoplanarity and $P_t/\sqrt{s}$ are used as well as the thrust T [24] of the event. The event is forced to form four jets. The smallest number of tracks in any jet is denoted $N^{\text{min}}_{\text{ch,j4}}$, and the variables $\theta^{\text{min}}_{\text{j4}}$ and $\theta^{\text{max}}_{\text{j4}}$ represent the smallest and largest angle between any two jets.

The discriminant variable $M_{\text{tot}}/\sqrt{s}$ is shown in Figs. 2c and 2d after the preselection and final selection respectively. In this subclass, the targeted-signal efficiency is 32% and the number of background events is 8.2.

5.3 Class 2: Final state with more than one hard lepton

5.3.1 Class 2a: Two leptons and four jets

targeted channel: $\mathrm{ZH} \to \ell^+\ell^-\,\mathrm{q\bar{q}}\,\mathrm{q\bar{q}}$

The dominant backgrounds after preselection are $\mathrm{q\bar{q}}$, semi-leptonic WW as well as ZZ events where one of the Z bosons decays into hadrons and the other into leptons. The rejection of $\mathrm{q\bar{q}}$ and WW events is achieved by applying a cut on the variable y_{45} and requiring the invariant mass of the two leptons ($m^{\text{rec}}_{\text{Z}}$) to be in a window around the nominal Z mass (m_{Z}). The remaining ZZ background is reduced by cutting on the angle between the two leptons and on their total energy. The details of the preselection and selection are shown in Table 6.

The discriminant variable, inspired from the Higgs boson mass is then computed as:

$$D_1 = \sqrt{(E_{\text{tot}} - E_{\ell_1} - E_{\ell_2})^2 - (\vec{P}_{\text{tot}} - \vec{P}_{\ell_1} - \vec{P}_{\ell_2})^2}\ , \tag{2}$$

where $\vec{P}_{\ell_1}$ and $\vec{P}_{\ell_2}$ are the momenta of the leptons associated with the selected pair and $\vec{P}_{\text{tot}}$ is the total measured momentum. The discriminant variable is shown in Figs. 3a and 3b after preselection and final selection, respectively. In this subclass, the targeted-signal efficiency is 74%. The expected background is 0.67 events.

5.3.2 Class 2t: Two leptons and missing energy

targeted channel: $\mathrm{ZH} \to \ell^+\ell^-\,\tau\nu\,\mathrm{q\bar{q}}$

This is the only case where the one- or three-prong hadronic tau decays can be distinguished efficiently from other hadronic decays. The rejection of $\mathrm{q\bar{q}}$ and WW events is achieved by requiring the reconstructed mass of the two leptons to be in a window around the Z mass. A cut on the transverse momentum of the lepton pair ($P_t(\ell^+\ell^-)$) reduces the ZZ background. The selection cuts are shown in Table 7. In this subclass, the targeted-signal efficiency is 60%. The expected background is 0.46 events.

5.3.3 Class 2b: Two leptons, two jets and one soft lepton

targeted channel: $\mathrm{ZH} \to \ell^+\ell^-\,\mathrm{q\bar{q}}\,\ell\nu$

This subclass is characterized by a third lepton and significant hadronic activity. The selection proceeds in a similar way as in the subclass 2a by concentrating on the two leptons associated with the Z boson decay. The isolation for the lepton that is the most anti-parallel to the missing momentum (I_{ℓ_A}) is used in the selection. The lepton tends to be more isolated in the signal than in the background. The selection cuts are shown in Table 8. After the final selection the dominant background is ZZ events decaying into $\ell^+\ell^-\mathrm{b\bar{b}}$.

The pair of leptons which have the same flavour and opposite charge and give the best estimate of the Z mass are associated with the Z boson decay. The following discriminant is used:

$$D_2 = \sqrt{(E_{\mathrm{tot}} - E_{\mathrm{Z}})^2 - (\vec{P}_{\mathrm{tot}} - \vec{P}_{\mathrm{Z}})^2 + 2(E_{\ell_3}(E_{\mathrm{tot}} - E_{\mathrm{Z}}) + \vec{P}_{\ell_3}(\vec{P}_{\mathrm{tot}} - \vec{P}_{\mathrm{Z}}))}\ , \qquad (3)$$

where $\vec{P}_{\mathrm{Z}}$ and E_{Z} are the momenta and energy of the Z boson, determined from the two assigned leptons. The additional term with respect to D_1 introduces the correction needed to take into account the undetected neutrino, assumed to be produced back-to-back to the third lepton. The discriminant variable is shown in Figs. 3c and 3d before and after the full selection, respectively. In this subclass, the targeted-signal efficiency is 71%. The expected background is 0.16 events.

5.3.4 Class 2c: Three leptons and two jets

targeted channel: $\mathrm{ZH} \to \ell^+\ell^-\,\ell\nu\,\mathrm{q\bar{q}}$

This subclass is characterized by a third lepton and low hadronic activity. Compared to subclass 2b, the missing transverse momentum is higher, which makes it more difficult to distinguish from semi-leptonic WW events. The mass window for the reconstructed Z mass is also broader due to the larger combinatorial background. A cut on the transverse momentum of the Z boson is applied to reduce the ZZ background.

The signal and background distributions of the discriminant variable, D_2, are shown in Figs. 3e and 3f. The dominant background is ZZ events. In this subclass, the targeted-signal efficiency is 91%. The expected background is 0.17 events.

5.3.5 Class 2d: Three leptons plus one track

targeted channel: $\mathrm{ZH} \to \ell^+\ell^-\,\ell\nu\,\ell\nu$

This subclass is characterized by a small branching fraction (the targeted channel represents 5% of the events in class 2) but with a clear topology: four leptons in the final state, one of them being soft. To reduce the ZZ background, cuts on the thrust and the event acoplanarity are applied. The remaining WW events are rejected by requiring that the most anti-parallel lepton with respect to the missing momentum is well isolated. The

selection criteria are detailed in Table 10. In this subclass, the targeted-signal efficiency is 57%. The expected background is 0.58 events.

5.4 Class 3: Final state with one hard lepton

In class 3, in order to reduce the $\gamma\gamma$ background, additional preselection cuts are applied on the total transverse momentum and on the cosine of the polar angle of the missing momentum $\cos(\theta_{\text{miss}})$. Depending on the subclass, a cut on the number of tracks and/or on the most energetic reconstructed photon (E_{γ_1}) is required.

5.4.1 Class 3a: One lepton and four jets

targeted channel: $\text{ZH} \to \text{q}\bar{\text{q}}\,\ell\nu\,\text{q}\bar{\text{q}}$

To eliminate the $\gamma\gamma$, $\ell^+\ell^-$ and $\text{q}\bar{\text{q}}$ backgrounds, cuts are applied to the track multiplicity, the angle between the hard lepton and the total momentum $\theta_{\ell,\Sigma}$, and the mass of the hard W boson, reconstructed as the invariant mass of the hard lepton and the missing momentum ($M_{\ell,P_{\text{miss}}}$). To suppress the remaining backgrounds, mainly WW, E_{ℓ_1}, the hadronic acollinearity ($\theta_{\text{aco (no lept)}}$) the thrust computed without the hard lepton ($T_{\text{no lept}}$), y_{45}, and the total transverse momentum are used. The selection criteria together with the numbers of signal, background and data events are summarized in Table 11.

Figures. 4a and 4b show the discriminant variable, $M_{\text{tot (hadr)}}$, after the preselection and after all cuts, respectively. In this subclass, the targeted-signal efficiency is 39%. The expected background is 2.9 events.

5.4.2 Class 3b: One lepton, two jets plus one soft lepton

targeted channel: $\text{ZH} \to \text{q}\bar{\text{q}}\,\ell\nu\,\ell\nu$

The selection procedure is very similar to that in subclass 3a, and is shown together with the numbers of signal, background and data events after each selection step in Table 12. The $\gamma\gamma$, $\ell^+\ell^-$ and $\text{q}\bar{\text{q}}$ backgrounds are rejected by cuts on the number of tracks, on the total acollinearity and on the transverse momentum. To further suppress $\text{q}\bar{\text{q}}$ events, cuts on the angle between the hard lepton and the total momentum as well as on the event sphericity are applied. Finally, most of the WW events are removed by a cut on the hard lepton energy which is sensibly smaller for signal events than for WW events, on the hadronic acollinearity, on $y_{12\ \text{(no lept)}}$, computed without the leptons, and on y_{34}. Remaining background events are mainly semi-leptonic WW decays with a soft lepton produced in a jet.

A good estimate of the Higgs boson mass can be obtained from twice the sum of the lepton energies. The following variable is therefore used as discriminant variable:

$$D_3 = 2(E_{\ell_1} + E_{\ell_2}). \tag{4}$$

The discriminant variable, D_3, after the preselection and after all cuts is shown in Figs. 4c and 4d respectively. In this subclass, the targeted-signal efficiency is 60%. The expected background is 0.76 events.

5.4.3 Class 3c: One lepton and one track

targeted channel: $\mathrm{ZH} \to \nu\bar{\nu}\,\ell\nu\,\ell\nu$

This subclass is characterized by a significant acollinearity between the two leptons, and by a small invariant mass. Only events with exactly two tracks are kept. The $\gamma\gamma$ events are rejected by a cut on the acollinearity and on the transverse momentum. The total mass and the acoplanarity are used to reject $\ell^+\ell^-$ events as well as part of the WW background. A final cut on the total missing mass and on $\theta_{\ell,\Sigma}$ removes most of the remaining WW and ZZ background.

The discriminant variable, D_3, after the preselection and after all cuts is given in Figs. 5a and 5b respectively. The selection criteria together with the numbers of signal, background and data events are summarized in Table 13. In this subclass, the targeted-signal efficiency is 58%. The expected background is 3.5 events.

5.4.4 Class 3d: One lepton and two jets

targeted channel: $\mathrm{ZH} \to \nu\bar{\nu}\,\ell\nu\,\mathrm{q\bar{q}}$

Events in this subclass are characterized by a single hard lepton with some soft hadronic activity. The $\gamma\gamma$ and $\ell^+\ell^-$ events are rejected by cutting on the aplanarity, A [24]. The dominant WW background is then reduced in two stages. First, the angle between the hard lepton and the total momentum and the energy of both the first and second most energetic leptons are used. Then, a final rejection is achieved by cuts on the sphericity, on $M_{\mathrm{tot\ (hadr)}}$ and on $y_{12\ \mathrm{(no\ lept)}}$.

The hadronic activity is included in the discriminant variable, defined as

$$D_4 = \sqrt{(E_{\mathrm{tot}} + E_{\ell_1})^2 - (\vec{P}_{\mathrm{tot}} - \vec{P}_{\ell_1})^2}. \tag{5}$$

The discriminant variable after the preselection and after all cuts is shown in Figs. 5c and 5d respectively. The selection criteria together with the numbers of signal, background and data events are summarized in Table 14. In this subclass, the targeted-signal efficiency is 58%. The expected background is 0.65 events.

5.5 Class 4: Soft-lepton final state

5.5.1 Class 4a: One soft lepton and four jets

targeted channel: $\mathrm{ZH} \to \mathrm{q\bar{q}}\,\mathrm{q\bar{q}}\,\ell\nu$

The event selection relies on y_{45}, $y_{34\ \mathrm{(no\ lept)}}$ and the lepton isolation, computed for the most anti-parallel lepton with respect to the missing momentum. This last variable

reduces the background by a factor 6 (for a 42% efficiency in signal events). A χ^2 is then built which takes into account the W and Z boson masses, reconstructed from the four jets in the event. For this, jets are paired and the mass of each pair is compared either to the nominal W boson mass or to the nominal Z boson mass. The jet pairing that minimizes the χ^2 is retained:

$$\chi^2 = \frac{(M_{12} - m_{\mathrm{Z}})^2}{\sigma^2} + \frac{(M_{34} - m_{\mathrm{W}})^2}{\sigma^2}, \tag{6}$$

were M_{12} and M_{34} are the masses of each jet pair and σ is the estimated mean resolution on the reconstructed mass. The background is finally reduced by constraining the value of the χ^2, the total hadronic mass and the lepton energy. The discriminating variable used for the estimation of the quoted confidence level is the reconstructed off-shell W mass, estimated from the missing momentum and the soft lepton momentum as follows:

$$D_5 = \sqrt{(E_{\mathrm{miss}} + E_{\ell_1})^2 - (P_{\mathrm{miss}} + \vec{P}_{\ell_1})^2}. \tag{7}$$

Details of the event selection are given in Table 15. The discriminant variable, after the preselection and the final selection is presented in Figs. 6a and 6b, respectively. In this subclass, the targeted-signal efficiency is 35%. The expected background is 4.0 events.

5.5.2 Class 4b: One soft lepton and two jets

targeted channel: $\mathrm{ZH} \to \nu\bar{\nu}\,\mathrm{q\bar{q}}\,\ell\nu$

Events are selected by cutting on y_{12} and y_{34}, on the number of tracks and on the lepton energy. The remaining background, still 75 times larger than the signal, is reduced by additional cuts on the total hadronic mass, the lepton isolation and on the hadronic acollinearity. Since at least three neutrinos are expected in this channel, a cut on the missing mass is used in the final selection. The dominant background after the selection is WW.

The discriminant variable, D_5, after the preselection and the final selection is presented in Figs. 6c and 6d, respectively. The expected number of events after the signal selection is shown in Table 16. In this subclass, the targeted-signal efficiency is 54%. The expected background is 8.0 events.

6 Results

The numbers of signal ($m_{\mathrm{H}} = 110\,\mathrm{GeV}/c^2$), background and data events for the years 1999 and 2000, for each class, are given in Table 17. The numbers of observed events agree well with the expectations for all subclasses but 3a and 3c, where there is a small excess ($\sim 2\sigma$) over the expected background ($\mathrm{CL_b}$=0.97). For subclass 3a, 6.6 background events remain after the cuts, for 1.27 signal events, while thirteen candidates are observed. Similarly, for subclass 3c, 0.15 signal events are expected for 6.6 background events, and fourteen

candidates are observed in the data. The best sensitivity is achieved for subclasses with a low expected $\langle \mathrm{CL_s} \rangle$. These are subclasses 3d, 3a, 4a, 2a and 1b, in that order.

The four classes are combined and the compatibility between data and background with and without the signal is evaluated with the log-likelihood ratio estimator $\ln \mathrm{Q}$ [23]. The combined expected values of the signal and background confidence levels are 0.08 and 0.50 respectively. The observed values for the signal and background confidence levels are 0.26 and 0.87, respectively.

6.1 Systematic uncertainties

The main contribution to the systematic error comes from the simulated statistics. The uncertainties from the production cross sections, from the simulation of the calorimeter energy scale and from hadronization processes are also taken into account. The beam background is conservatively taken into account in the analysis (via event selection variable E_{12}). Uncertainties from the simulated statistics are included when combining the searches in the several subclasses by varying the expected signal and background levels bin per bin in a number of toy Monte Carlo experiments, while other uncertainties are taken into account in a correlated way by varying the expected signal and background levels coherently in the same direction for all subclasses and all bins. Each source of uncertainty is nevertheless handled independently, which corresponds to adding up their effect in quadrature.

For the four different classes, after applying the selection cuts, the main remaining background comes from WW pair production. The related uncertainty, associated to W decays into three jets, is taken to be 2%. This is a conservative estimate from the uncertainty on the α_s measurement [25]. The systematic errors related to the simulation of the absolute energy scale of the calorimeters are determined using hadronic Z events and are found to be $\pm 0.9\%$ and $\pm 2\%$ for the electromagnetic and hadronic calorimeters, respectively. The effect of a possible miscalibration of the calorimeters is evaluated on simulated samples by scaling the electromagnetic and hadronic part of the measured energy independently by these amounts. The largest of the observed shifts for each calorimeter is combined in quadrature. This leads to a mean uncertainty of the order of 3% on the remaining background level. The uncertainties originating from the hadronization model are evaluated by comparing WW events hadronized using the string model (`JETSET 7.4` [26] Monte Carlo) and with the colour dipole model (`ARIADNE 4.10` [27] Monte Carlo). The associated mean systematic error is 6%. Both the hadronization and calorimetric uncertainties are evaluated separately for each subclass. The uncertainties taken into account are presented in Table 18.

6.2 Combined Likelihood Ratio

The combined log-likelihood ratio as a function of the Higgs boson mass is presented in Fig. 7. A 1.5σ excess is observed. This excess does not depend on the hypothetical mass,

and no supporting indication of a signal is seen. An upper limit on the signal cross section is set as a function of the Higgs boson mass.

6.3 Cross section upper limits

For each class in the analysis, an upper limit on the production cross section at a given Higgs boson mass is derived. Figure 8 presents the resulting 95% C.L. upper limit on $\xi^2 = \mathrm{BR}(\mathrm{H} \to \mathrm{WW})\sigma(\mathrm{e^+e^-} \to \mathrm{Hf\bar{f}})/\sigma^{\mathrm{SM}}(\mathrm{e^+e^-} \to \mathrm{Hf\bar{f}})$, as a function of the Higgs boson mass. The third class, providing the best compromise between a clean signature and signal sensitivity has the highest reach. The other three classes are nevertheless as important in order to get a competitive limit. Combining all four analyses, the 95% C.L. upper limit on ξ^2 as a function of the Higgs boson mass is given in Fig. 9. The benchmark fermiophobic Higgs model is drawn as the full line in the figure. The afore-mentioned excess in class 3 results in an observed limit which is less than the expected limit.

6.4 Mass exclusion limits

Lower limits on the Higgs boson mass can be extracted in the context of a given model from upper limits on the cross section presented in the previous section. If the branching ratio of the Higgs boson to W bosons is taken to be 100%, the expected limit is $107.5\,\mathrm{GeV}/c^2$. In the fermiophobic Higgs boson scenario, it is expected that Higgs boson masses between $97.5\,\mathrm{GeV}/c^2$ and $104\,\mathrm{GeV}/c^2$ can be excluded. For these two scenarios, due to the excess observed, no limit at 95% C.L. can be set.

However, the present search for $\mathrm{H} \to \mathrm{WW}$ can be combined with the previously published ALEPH search for $\mathrm{H} \to \gamma\gamma$ [4] to significantly improve the limits on the fermiophobic Higgs boson scenario (Fig. 1). The combined expected limit on the fermiophobic Higgs boson mass is $111.4\,\mathrm{GeV}/c^2$, an improvement of $\sim 7\,\mathrm{GeV}/c^2$ on the sensitivity from the $\mathrm{H} \to \gamma\gamma$ search alone [4][1]. The observed limit is $105.8\,\mathrm{GeV}/c^2$.

A model-independent limit can be derived by scanning the $\mathrm{H} \to \gamma\gamma$ and $\mathrm{H} \to \mathrm{WW}$ branching fractions. This is conveniently parametrized as:

$$\begin{aligned} \mathrm{BR}_{\mathrm{bosons}} &= \mathrm{BR}_{\mathrm{H}\to\gamma\gamma} + \mathrm{BR}_{\mathrm{H}\to\mathrm{WW}} + \mathrm{BR}_{\mathrm{H}\to\mathrm{ZZ}}, \\ \mathrm{R}_{\gamma\gamma} &= \mathrm{BR}_{\mathrm{H}\to\gamma\gamma}/\mathrm{BR}_{\mathrm{bosons}}, \end{aligned}$$

where $\mathrm{R}_{\gamma\gamma}$ represents the fraction of bosonic decays into photon pairs and ranges from zero to one. The best limit is obtained combining the present results with those previously published by ALEPH on the search for $\mathrm{H} \to \gamma\gamma$ [4]. The 95% C.L. limit on $\mathrm{BR}_{\mathrm{bosons}}$ is determined at each point of the m_{H} versus $\mathrm{R}_{\gamma\gamma}$ plane, resulting in the exclusion curves of Fig. 10.

[1]The actual expected limit quoted in Reference [4], $105.4\,\mathrm{GeV}/c^2$, results from using a definition of $\mathrm{CL_s}$ [22] which is different from the definition adopted in the present paper.

7 Conclusions

A search for a Higgs boson produced in association with a Z and decaying into a WW pair has been performed with a dataset of 453.2 pb^{-1} recorded by the ALEPH detector at centre-of-mass energies from 191 to 209 GeV. No statistically significant evidence for a fermiophobic Higgs boson decaying into a WW pair has been found in the data. Assuming Standard Model couplings to gauge bosons, a 95% C.L. upper limit on the ratio $\mathrm{BR}(\mathrm{H} \to \mathrm{WW})\sigma(\mathrm{e^+e^-} \to \mathrm{Hf\bar{f}})/\sigma^{\mathrm{SM}}(\mathrm{e^+e^-} \to \mathrm{Hf\bar{f}})$ has been obtained. Combining this analysis with the study of $\gamma\gamma$ decays of a Higgs boson [4], a Higgs boson mass up to $105.8\,\mathrm{GeV}/c^2$ has been excluded in the context of the benchmark fermiophobic scenario. A model-independent limit has been derived by scanning the $\mathrm{H} \to \gamma\gamma$ and $\mathrm{H} \to \mathrm{WW}$ branching fractions. This analysis complements existing searches for new physics beyond the Standard Model and constrains models introducing anomalous couplings in the Higgs sector.

Acknowledgments

It is a pleasure to congratulate our colleagues from the accelerator divisions for the outstanding operation of LEP 2, especially in its last year of running during which the accelerator performance was pushed beyond expectation. We are indebted to the engineers and technicians in all our institutions for their contributions to the excellent performance of the ALEPH detector. Those of us from non-member states wish to thank CERN for its hospitality and support.

References

[1] P.W. Higgs, Phys. Lett. **12** (1964) 132; F. Englert and R. Brout, Phys. Rev. Lett. **13** (1964) ; G. Guralnik and C.K. Hagen, Phys. Rev. Lett. **13** (1964) 585; T.W.B. Kibble, Phys. Rev. **155** (1967) 1554.

[2] A.G. Akeroyd, Phys. Lett. **B368** (1996) 89; H. Haber, G. Kane and T. Sterling, Nucl. Phys. **B161** (1979) 493.

[3] K. Hagiwara, R. Szalapki and D. Zeppenfeld, Phys. Lett. **B318** (1993) 155.

[4] ALEPH Coll., A. Heister et al., "Search for $\gamma\gamma$ Decays of a Higgs Boson in $\mathrm{e^+e^-}$ Collisions at $\sqrt{s}$ up to 209 GeV", Phys. Lett. **B544** (2002) 16.

[5] DELPHI Coll., "Search for Fermiophobic Higgs Bosons in Final States with Photons at LEP 2", Eur. Phys. J. **C35** (2004) 313.

[6] L3 Coll., P. Achard et al., "Search for a Higgs Boson Decaying into Two-Photons at LEP", Phys. Lett. **B534** (2002) 28.

[7] OPAL Coll., G. Abbiendi et al., "Search for Associated Production of Massive States Decaying into Two Photons in e^+e^- Annihilation at $\sqrt{s}$=88-209 GeV", Phys. Lett. **B544** (2002) 44.

[8] The ALEPH, DELPHI, L3 and OPAL Collaborations, The LEP Higgs Working Group, The LEP Higgs Working Group, Searches for Higgs Bosons Decaying into Photons: Combined Results from the LEP experiments, LHWG Note 2002-02. Contributed paper for ICHEP'02. Amsterdam, July 2002.

[9] G. Ganis and P. Janot, "The HZHA Generator" in "Physics at LEP2", Eds. G. Altarelli, T. Sjöstrand and F. Zwirner, CERN 96-01 (1996), Vol 2, 309.

[10] L3 Coll., P. Achard et al., "Search for a Higgs Boson Decaying to Weak Boson Pairs at LEP", Phys. Lett. **B568** (2003) 191.

[11] ALEPH Coll., D. Décamp et al., "ALEPH: A Detector for Electron-Positron Annihilations at LEP", Nucl. Instrum. and Methods **A294** (1990) 121; D. Creanza et al., "The new ALEPH vertex detector", Nucl. Instrum. and Methods **A409** (1998) 157.

[12] ALEPH Coll., D. Buskulic et al., "Performance of the ALEPH Detector at LEP", Nucl. Instrum. and Methods **A360** (1995) 481.

[13] ALEPH Coll., S. Schael et al., "Measurement of W-pair production in e^+e^- collisions at centre-of-mass energies from 183 to 209 GeV", CERN-EP-PH-2004-012, Eur. Phys. J. **C38** (2004) 147-160.

[14] S. Catani et al., Phys. Lett. **B269** (1991) 432.

[15] Tomasz Pierzchala, Private communication.

[16] S. Jadach, W. Placzek and B.F.L. Ward, Phys. Lett. **B390** (1997) 298.

[17] S. Jadach, B.F.L. Ward and Z. Wąs, Comput. Phys. Commun. **130** (2000) 260.

[18] J.A.M. Vermaseren, in "Proceedings of the IVth International Workshop on Gamma Gamma interactions", Eds. G. Cochard and P. Kessler, Springer Verlag, 1980.

[19] S. Jadach et al., Comput. Phys. Commun. **140** (2001) 475.

[20] T. Sjöstrand et al., Comput. Phys. Commun. **135** (2001) 238.

[21] P. Janot and F. Le Diberder, "Optimally combined confidence limits", Nucl. Instrum. and Methods **A411** (1998) 435.

[22] S. Jin and P. McNamara, "The signal estimator limit setting method", Nucl. Instrum. and Methods **A462** (2001) 561.

[23] T. Junk, "Condence level computation for combining searches with small statistics", Nucl. Instrum. and Methods **A434** (1999) 435.

[24] S. Brandt et al., Phys. Lett. **12** (1964) 57; E. Farhi, Phys. Rev. Lett. **39** (1977) 1587.

[25] Particle Data Group, "Review of Particle Physics", Phys. Lett. **B592** (2004) 1.

[26] T. Sjöstrand, Comput. Phys. Commun. **67** (1994) 74.

[27] T. Sjöstrand, Comput. Phys. Commun. **71** (1992) 15.

Table 1: Integrated luminosities and centre-of-mass (CM) energy ranges for the data collected by the ALEPH detector for the years 1999 and 2000.

Year	Luminosity (pb^{-1})	CM energy (GeV)
2000	7.3 ± 0.05	$207 - 209$
	125.9 ± 0.6	$206 - 207$
	81.4 ± 0.4	$204 - 206$
1999	42.6 ± 0.2	$201 - 203$
	87.2 ± 0.4	199.5
	79.9 ± 0.4	195.5
	28.9 ± 0.1	191.6

Table 2: Search topologies and targeted final states (with corresponding branching fractions) in the four event classes. For the targeted final states, the Z, W, and W* decays are given in this order.

Class and topology	Targeted Channel	(BR)
1: Fully-Hadronic	**No leptonic decay**	**(0.422)**
1a: 6 jets	$\mathrm{q\bar{q}\,q\bar{q}\,q\bar{q}}$	(0.328)
1b: 4 jets and E_{miss}	$\nu\bar{\nu}\,\mathrm{q\bar{q}\,q\bar{q}}$	(0.094)
2: Two-Hard-Leptons	**Z leptonic decays**	**(0.054)**
2a: plus jets	$\ell^+\ell^-\,\mathrm{q\bar{q}\,q\bar{q}}$	(0.032)
2t: plus jets and E_{miss}	$\ell^+\ell^-\,\tau\nu\,\mathrm{q\bar{q}}$	(0.003)
2b: plus jets and 1 soft lepton	$\ell^+\ell^-\,\mathrm{q\bar{q}}\,\ell\nu$	(0.010)
2c: plus jets and 1 hard lepton	$\ell^+\ell^-\,\ell\nu\,\mathrm{q\bar{q}}$	(0.007)
2d: plus 1 hard lepton and 1 track	$\ell^+\ell^-\,\ell\nu\,\ell\nu$	(0.003)
3: One-Hard-Lepton (and E_{miss})	**W leptonic decays**	**(0.171)**
3a: plus jets	$\mathrm{q\bar{q}}\,\ell\nu\,\mathrm{q\bar{q}}$	(0.101)
3b: plus jets and 1 soft lepton	$\mathrm{q\bar{q}}\,\ell\nu\,\ell\nu$	(0.031)
3c: plus 1 track and M_{miss}	$\nu\bar{\nu}\,\ell\nu\,\ell\nu$	(0.029)
3d: plus jets and M_{miss}	$\nu\bar{\nu}\,\ell\nu\,\mathrm{q\bar{q}}$	(0.008)
4: One-Soft-Lepton	**W* leptonic decays**	**(0.130)**
4a: plus jets	$\mathrm{q\bar{q}\,q\bar{q}}\,\ell\nu$	(0.101)
4b: plus jets and M_{miss}	$\nu\bar{\nu}\,\mathrm{q\bar{q}}\,\ell\nu$	(0.029)

Table 3: Details of the partition of events into each of the thirteen subclasses. Energies are expressed in GeV and masses in GeV/c^2.

Subclass	Selection Criteria							
	E_{ℓ_1}	E_{ℓ_2}	E_{ℓ_3}	D_{14}	$M_{\rm tot}/\sqrt{s}$	$M_{\rm miss}$	$E_{\rm had}$	$N_{\rm ch}$
1a	< 25			< 13		< 60		
1b	< 25			< 13		> 60		
2a	> 25	> 20	< 8				> 60	
2t	> 25	> 20	< 8				< 60	
2b	> 25	> 20	> 8				> 60	
2c	> 25	> 20	> 8				< 60	> 4
2d	> 25	> 20	> 8				< 60	$= 4$
3a	> 25	< 10			> 0.4	< 95		
3b	> 25	$[10, 20]$			> 0.4	< 95		
3c	> 25	$[10, 20]$			< 0.4	> 95		
3d	> 25	< 10			< 0.4	> 95		
4a	< 25			> 13	> 0.6			
4b	< 25			> 13	< 0.6			

Table 4: Selection criteria for each subclass in subclass 1a. The numbers of signal ($N_{\rm s}$), background ($N_{\rm b}$) and data ($N_{\rm d}$) events are given in the table for the year 2000. Energies, momenta and masses are expressed in GeV, GeV/c and GeV/c^2, respectively.

Subclass 1a	Cuts	$N_{\rm s}$	$N_{\rm b}$	$N_{\rm d}$
Preselection	$N_{\rm ch} > 25$			
	$M_{\rm tot}/\sqrt{s} > 0.6$			
	$P_l/\sqrt{s} < 0.15$			
	$0.1 < S < 0.85$			
	$\ln(y_{34}) > -5.3$	10.9	1452.0	1401
Topological	$S > 0.13$	10.7	1374.1	1325
	$N_{\rm ch} > 32$	9.17	866.9	845
	$\ln(y_{56}) > -7.2$	8.18	494.5	481
	$\ln(y_{12} + y_{34} + y_{56}) > -0.83$	8.07	476.4	456
	$N^{\rm min}_{\rm ch,j6} > 0$	6.28	231.5	247
	$(\theta^{\rm min}_{\rm j6} + \theta^{\rm max}_{\rm j6}) > 190.^\circ$	6.21	212.3	229
Masses	$M_1 < 117.$	6.10	186.7	200
	$M_3 > 13.$	5.74	163.7	168

Table 5: Selection criteria for each subclass in subclass 1b. The numbers of signal (N_s), background (N_b) and data (N_d) events are given in the table for the year 2000. Energies, momenta and masses are expressed in GeV, GeV/c and GeV/c^2, respectively.

Subclass 1b	Cuts	N_s	N_b	N_d
Preselection	$\cos(\theta_\mathrm{miss}) < 0.9$			
	$E_{12} < 0.05$			
	$N_\mathrm{ch} > 12$			
	$M_\mathrm{tot}/\sqrt{s} > 0.35$			
	$P_l/\sqrt{s} < 0.2$			
	$0.03 < S < 0.8$			
	$\ln(y_{34}) > -7.6$	3.60	190.4	211
Topological	$N_\mathrm{ch} > 24$	1.77	31.2	46
	$\ln(y_{34}) > -6.6$	1.73	28.2	43
Anti-q$\bar{\mathrm{q}}$	$\Phi_\mathrm{aco} < 179.$	1.69	26.1	38
	$P_t/\sqrt{s} > 0.035$	1.63	22.0	28
Anti-WW	$T > 0.74$	1.33	16.3	23
	$P_l/\sqrt{s} < 0.12$	1.25	12.1	19
	$N^\mathrm{min}_\mathrm{ch,j4} > 0$	1.23	11.3	18
	$\theta^\mathrm{min}_\mathrm{j4} > 23.^\circ$	1.16	8.61	15
	$(\theta^\mathrm{min}_\mathrm{j4} + \theta^\mathrm{max}_\mathrm{j4}) > 170.^\circ$	1.11	8.18	13

Table 6: Selection criteria for each subclass in subclass 2a. The numbers of signal (N_s), background (N_b) and data (N_d) events are given in the table for the year 2000. Energies, momenta and masses are expressed in GeV, GeV/c and GeV/c^2, respectively.

Subclass 2a	Cuts	N_s	N_b	N_d
Preselection	$N_\mathrm{ch} > 8$	1.03	48.8	39
Anti-q$\bar{\mathrm{q}}$, WW	$\ln(y_{45}) \geq -7.$			
	$\lvert m^\mathrm{rec}_\mathrm{Z} - m_\mathrm{Z}\rvert < 14.$	0.62	6.29	2
Anti-ZZ	$\theta_{\ell_1\ell_2} > 135.^\circ$			
	$E_{\ell_1} + E_{\ell_2} < 95.$	0.54	0.67	2

Table 7: Selection criteria for each subclass in subclass 2t. The numbers of signal (N_s), background (N_b) and data (N_d) events are given in the table for the year 2000. Energies, momenta and masses are expressed in GeV, GeV/c and GeV/c^2, respectively.

Subclass 2t	Cuts	N_s	N_b	N_d
Preselection	$P_t/\sqrt{s} > 0.002$	0.08	2.59	2
Selection	$\lvert m^\mathrm{rec}_\mathrm{Z} - m_\mathrm{Z}\rvert < 23.$			
	$P_t(\ell^+\ell^-) < 60.$	0.06	0.46	1

Table 8: Selection criteria for each subclass in subclass 2b. The numbers of signal ($N_{\rm s}$), background ($N_{\rm b}$) and data ($N_{\rm d}$) events are given in the table for the year 2000. Energies, momenta and masses are expressed in GeV, GeV/c and GeV/c^2, respectively.

Subclass 2b	Cuts	$N_{\rm s}$	$N_{\rm b}$	$N_{\rm d}$
Preselection	$N_{\rm ch} > 7$	0.29	10.7	12
Anti-q$\bar{\rm q}$, WW	$\ln(y_{45}) > -8.$ $\lvert m_{\rm Z}^{\rm rec} - m_{\rm Z}\rvert < 20.$ $\ln(I_{\ell_A}) > -7.$	0.19	1.08	0
Anti-ZZ	$\theta_{\ell_1\ell_2} > 142.^\circ$ $E_{\ell_1} + E_{\ell_2} < 98.$	0.18	0.16	0

Table 9: Selection criteria for each subclass in subclass 2c. The numbers of signal ($N_{\rm s}$), background ($N_{\rm b}$) and data ($N_{\rm d}$) events are given in the table for the year 2000. Energies, momenta and masses are expressed in GeV, GeV/c and GeV/c^2, respectively.

Subclass 2c	Cuts	$N_{\rm s}$	$N_{\rm b}$	$N_{\rm d}$
Preselection	$P_t/\sqrt{s} > 0.01$ $N_{\rm ch} > 4$	0.23	1.73	2
Anti-q$\bar{\rm q}$, WW	$\ln(y_{45}) > -11.$ $\lvert m_{\rm Z}^{\rm rec} - m_{\rm Z}\rvert < 23.$ $\ln(I_{\ell_A}) > -11.$	0.20	0.18	0
Anti-ZZ	$P_{t_{\rm Z}} < 60.$	0.20	0.17	0

Table 10: Selection criteria for each subclass in subclass 2d. The numbers of signal ($N_{\rm s}$), background ($N_{\rm b}$) and data ($N_{\rm d}$) events are given in the table for the year 2000. Energies, momenta and masses are expressed in GeV, GeV/c and GeV/c^2, respectively.

Subclass 2d	Cuts	$N_{\rm s}$	$N_{\rm b}$	$N_{\rm d}$
Preselection	$P_t/\sqrt{s} > 0.11$	0.10	3.13	3
Anti-ZZ	$T < 0.98$ $\Phi_{\rm aco} < 176.^\circ$	0.09	0.93	1
Anti-WW	$\ln(I_{\ell_A}) > -9.$	0.09	0.58	0

Table 11: Selection criteria for each subclass in subclass 3a. The numbers of signal ($N_{\rm s}$), background ($N_{\rm b}$) and data ($N_{\rm d}$) events are given in the table for the year 2000. Energies, momenta and masses are expressed in GeV, GeV/c and GeV/c^2, respectively.

Subclass 3a	Cuts	$N_{\rm s}$	$N_{\rm b}$	$N_{\rm d}$
Preselection	$P_t/\sqrt{s} > 0.05$ $\lvert\cos(\theta_{\rm miss})\rvert < 0.9$ $N_{\rm ch} > 3$	2.7	793.4	823
Anti-q$\bar{\rm q}$, $\ell\ell$, $\gamma\gamma$	$N_{\rm ch} > 20$ $\theta_{\ell,\Sigma} < 41.^\circ$ $M_{\ell,P_{\rm miss}} > 55.$	1.57	37	43
Anti-WW	$E_{\ell_1} < 55.$ $\theta_{\rm aco\ (no\ lept)} > 137.^\circ$ $T_{\rm no\ lept} < 0.93$	1.42	5.7	12
Anti-WW	$\ln(y_{45}) > -7.2$ $P_t/\sqrt{s} < 0.25$	1.24	2.9	5

Table 12: Selection criteria for each subclass in subclass 3b. The numbers of signal ($N_{\rm s}$), background ($N_{\rm b}$) and data ($N_{\rm d}$) events are given in the table for the year 2000. Energies, momenta and masses are expressed in GeV, GeV/c and GeV/c^2, respectively.

Subclass 3b	Cuts	$N_{\rm s}$	$N_{\rm b}$	$N_{\rm d}$
Preselections	$P_t/\sqrt{s} > 0.05$ $\lvert\cos(\theta_{\rm miss})\rvert < 0.9$ $N_{\rm ch} > 3$ $E_{\gamma_1} < 40.$	0.85	86.96	86
Anti-q$\bar{\rm q}$, $\ell\ell$, $\gamma\gamma$	$N_{\rm ch} > 5$ $\theta_{\rm aco} < 178.^\circ$ $P_t/\sqrt{s} > 0.08$	0.79	55.40	52
Anti-q$\bar{\rm q}$	$\theta_{\ell,\Sigma} < 41.^\circ$ $\ln(S) > -2.2$	0.59	3.63	5
Anti-WW	$E_{\ell_1} < 55.$ $\theta_{\rm aco\ (no\ lept)} > 135.^\circ$ $y_{12\ \rm (no\ lept)} > 0.23$ $\ln(y_{34}) > -6.$	0.49	0.76	1

Table 13: Selection criteria for each subclass in subclass 3c. The numbers of signal ($N_{\rm s}$), background ($N_{\rm b}$) and data ($N_{\rm d}$) events are given in the table for the year 2000. Energies, momenta and masses are expressed in GeV, GeV/c and GeV/c^2, respectively.

Subclass 3c	Cuts	$N_{\rm s}$	$N_{\rm b}$	$N_{\rm d}$
Preselections	$P_t/\sqrt{s} > 0.05$ $\lvert\cos(\theta_{\rm miss})\rvert < 0.9$ $E_{\gamma_1} < 15.$	0.17	19.9	20
Anti-$\gamma\gamma$	$N_{\rm ch} = 2$ $\theta_{\rm aco} < 138.^\circ$ $P_t/\sqrt{s} > 0.09$	0.15	11.16	14
Anti-$\ell\ell$, WW	$M_{\rm tot}/\sqrt{s} < 0.26$ $\Phi_{\rm aco} < 160.^\circ$	0.14	7.9	9
Anti-WW, ZZ	$M_{\rm miss} > 127.$ $\theta_{\ell,\Sigma} < 32.^\circ$	0.12	3.5	5

Table 14: Selection criteria for each subclass in subclass 3d. The numbers of signal ($N_{\rm s}$), background ($N_{\rm b}$) and data ($N_{\rm d}$) events are given in the table for the year 2000. Energies, momenta and masses are expressed in GeV, GeV/c and GeV/c^2, respectively.

Subclass 3d	Cuts	$N_{\rm s}$	$N_{\rm b}$	$N_{\rm d}$
Preselections	$P_t/\sqrt{s} > 0.05$ $\lvert\cos(\theta_{\rm miss})\rvert < 0.9$ $N_{\rm ch} > 3$ $E_{\gamma_1} < 15.$	1.22	829.8	836
Anti-$\gamma\gamma, \ell\ell$	$\ln(A) > -8$	0.94	4.92	3
Anti-WW	$\theta_{\ell,\Sigma} < 57.^\circ$ $E_{\ell_1} < 60.$ $E_{\ell_2} < 6.$	0.90	3.39	1
Anti-WW	$-5. < \ln(S) < -2.$ $M_{\rm tot\ (hadr)}/\sqrt{s} < 0.17$ $\ln(y_{12\ \text{(no lept)}}) > -4.$	0.79	0.65	0

Table 15: Selection criteria for each subclass in subclass 4a. The numbers of signal ($N_{\rm s}$), background ($N_{\rm b}$) and data ($N_{\rm d}$) events are given in the table for the year 2000. Energies, momenta and masses are expressed in GeV, GeV/c and GeV/c^2, respectively.

Subclass 4a	Cuts	$N_{\rm s}$	$N_{\rm b}$	$N_{\rm d}$
Preselections	$N_{\rm ch} > 10$ $\vert\cos(\theta_{\rm miss})\vert < 0.95$	4.6	818	794
Group 1	$\ln(y_{45}) > -6.$ $\ln(y_{34\ \text{(no lept)}}) > -4.6$ $\ln(I_{\ell_A}) > -3.5$	1.4	7.4	8
Group 2	$\chi^2 < 0.02$ $M_{\text{tot (hadr)}}/\sqrt{s} < 0.95$ $E_{\ell_A} > 7.$	1.17	4.0	2

Table 16: Selection criteria for each subclass in subclass 4b. The numbers of signal ($N_{\rm s}$), background ($N_{\rm b}$) and data ($N_{\rm d}$) events are given in the table for the year 2000. Energies, momenta and masses are expressed in GeV, GeV/c and GeV/c^2, respectively.

Subclass 4b	Cuts	$N_{\rm s}$	$N_{\rm b}$	$N_{\rm d}$
Preselections	$N_{\rm ch} > 3$ $P_t/\sqrt{s} > 0.05$ $\vert\cos(\theta_{\rm miss})\vert < 0.95$	2.4	478	485
Group 1	$\ln(y_{12\ \text{(no lept)}}) > -7.$ $\ln(y_{23\ \text{(no lept)}}) > -2.6$ $N_{\rm ch} > 9$ $E_{\ell_A} > 7.$	1.35	99.7	82
Group 2	$M_{\text{tot (hadr)}} \in [50., 103.]$ $\ln(I_{\ell_A}) > -4.5$ $\theta_{\text{aco (no lept)}} > 140.^\circ$ $M_{\rm miss} > 65.$	0.69	8.0	5

Table 17: Numbers of signal events for a 110 GeV/c^2 Higgs boson (N_s), background (N_b) and data (N_d) events, as well as the value of the expected and observed confidence levels for each subclass, for the years 1999 and 2000 together.

Class	N_s	N_b	N_d	$\langle CL_s \rangle$	CL_s
1a : $ZH \to q\bar{q}\,q\bar{q}\,q\bar{q}$	6.80 ± 0.06	372.7 ± 1.7	360	0.60	0.50
1b : $ZH \to \nu\bar{\nu}\,q\bar{q}\,q\bar{q}$	1.35 ± 0.03	18.0 ± 0.4	20	0.58	0.79
Class 1 combined	8.15 ± 0.07	390.7 ± 1.7	380	0.44	0.53
2a : $ZH \to \ell^+\ell^-\,q\bar{q}\,q\bar{q}$	0.64 ± 0.02	2.41 ± 0.07	5	0.57	0.91
2t : $ZH \to \ell^+\ell^-\,\tau\nu\,q\bar{q}$	0.070 ± 0.006	1.21 ± 0.08	1	0.94	0.96
2b : $ZH \to \ell^+\ell^-\,q\bar{q}\,\ell\nu$	0.21 ± 0.01	0.57 ± 0.04	2	0.81	0.83
2c : $ZH \to \ell^+\ell^-\,\ell\nu\,q\bar{q}$	0.24 ± 0.01	0.31 ± 0.05	0	0.79	0.79
2d : $ZH \to \ell^+\ell^-\,\ell\nu\,\ell\nu$	0.113 ± 0.008	1.33 ± 0.12	1	0.91	0.90
Class 2 combined	1.27 ± 0.03	5.82 ± 0.17	9	0.43	0.73
3a : $ZH \to q\bar{q}\,\ell\nu\,q\bar{q}$	1.27 ± 0.03	6.6 ± 0.2	13	0.47	0.84
3b : $ZH \to q\bar{q}\,\ell\nu\,\ell\nu$	0.58 ± 0.02	2.01 ± 0.12	3	0.62	0.66
3c : $ZH \to \nu\bar{\nu}\,\ell\nu\,\ell\nu$	0.150 ± 0.009	6.6 ± 0.2	14	0.95	0.99
3d : $ZH \to \nu\bar{\nu}\,\ell\nu\,q\bar{q}$	0.89 ± 0.02	0.99 ± 0.15	1	0.44	0.43
Class 3 combined	2.89 ± 0.04	16.2 ± 0.4	32	0.23	0.47
4a : $ZH \to q\bar{q}\,q\bar{q}\,\ell\nu$	1.41 ± 0.03	8.92 ± 0.2	8	0.55	0.40
4b : $ZH \to \nu\bar{\nu}\,q\bar{q}\,\ell\nu$	0.85 ± 0.02	20.34 ± 0.4	19	0.78	0.68
Class 4 combined	2.27 ± 0.03	29.3 ± 0.5	27	0.50	0.30
All combined	14.6 ± 0.09	441.9 ± 1.9	448	0.08	0.26

Table 18: Levels of systematic uncertainties considered for each subclass. The corresponding total systematic uncertainty is also given in the last column, excluding the impact of the limited simulated statistics.

Subclass	Systematic uncertainty sources			
	Calorimetry	Hadronization	$W \to 3$ jets	Total
1a	0%	2%	2%	2.8%
1b	6%	8%	2%	10.2%
2	0%	0%	2%	2%
3a	2%	4%	2%	4.9%
3b	0%	14%	2%	14.1%
3c	2%	8%	2%	8.5%
3d	12%	8%	2%	14.6%
4a	2%	0%	2%	2.8%
4b	0%	9%	2%	9.2%

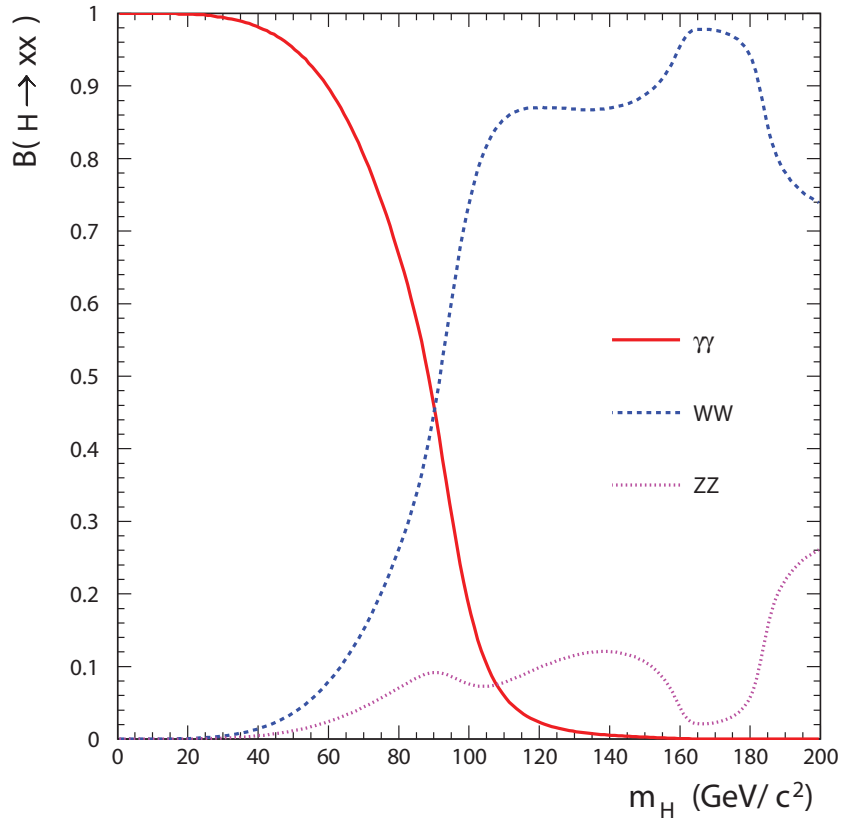

Figure 1: Branching fraction of benchmark fermiophobic Higgs boson (defined in the text) into boson pairs as calculated by `HZHA` [9].

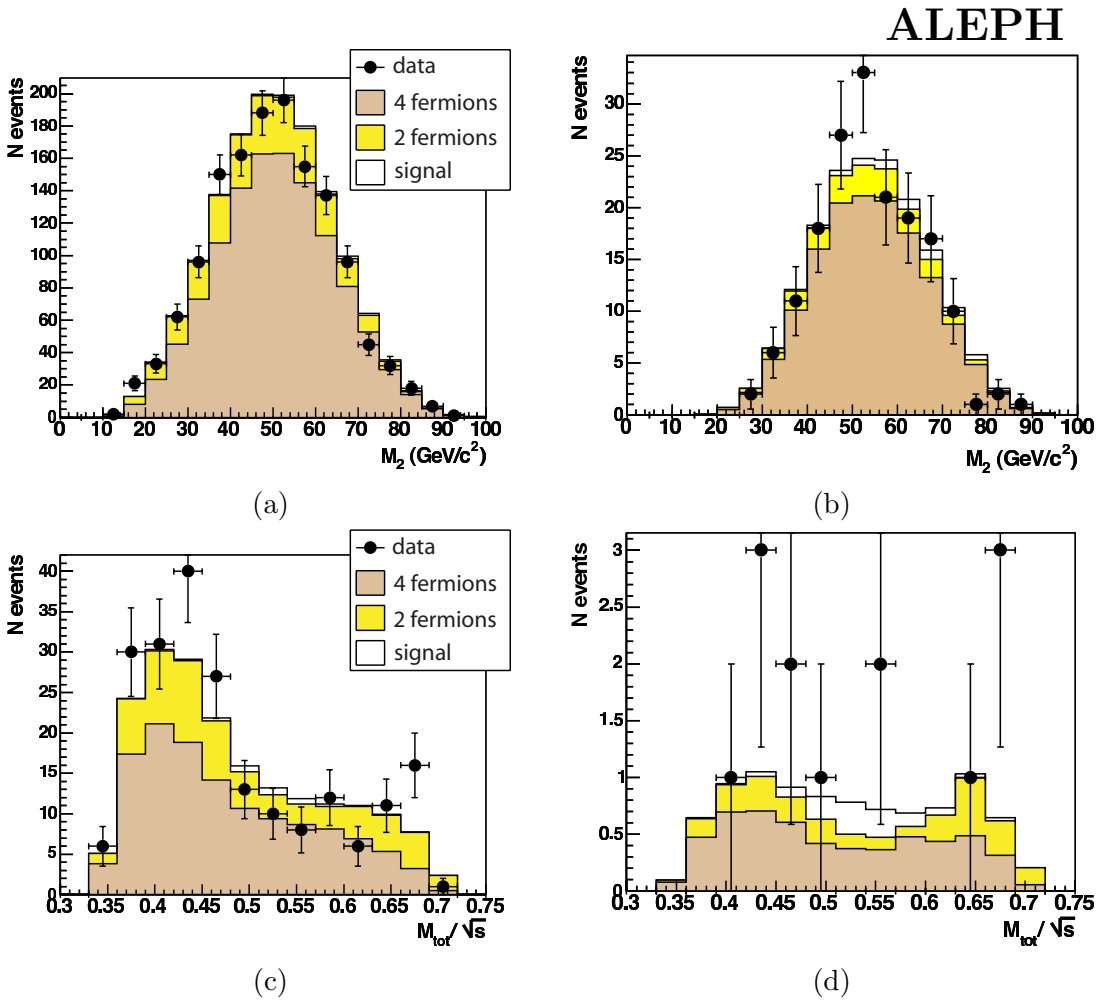

Figure 2: Discriminant variable M_2 for class 1a events after the preselection (a) and after the final selection cuts (b). Discriminant variable $M_{\rm tot}/\sqrt{s}$ for class 1b events after the preselection (c) and after the final selection cuts (d). All distributions are obtained from year 2000 data.

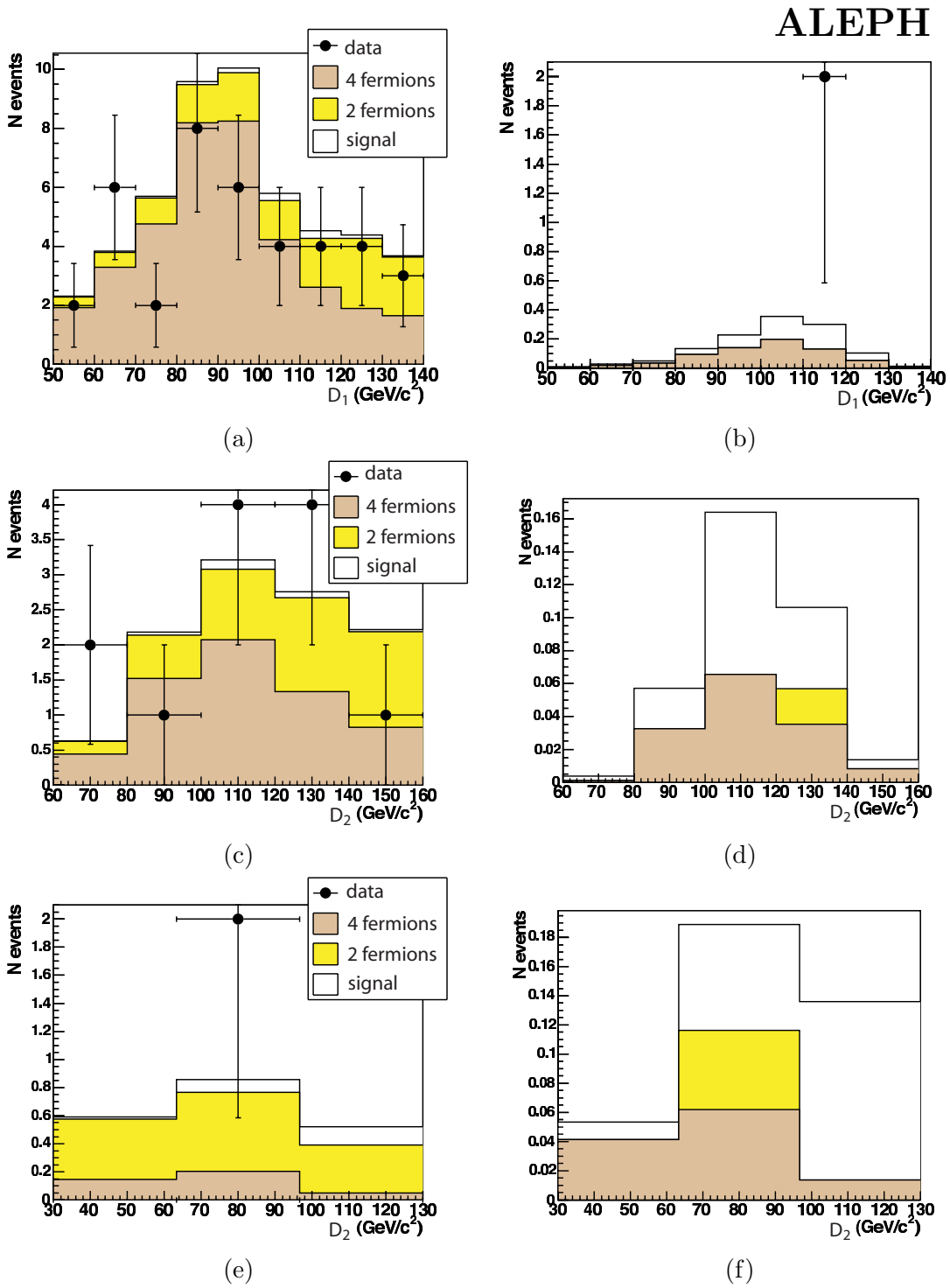

Figure 3: Discriminant variable, D_1, for subclass 2a after the preselection (a) and the final selection (b). In plots (c) and (d), the discriminant variable, D_2, is shown after the preselection and the final selection, respectively, for events in class 2b. The two lower plots (e) and (f) show the same variable, after the preselection and the final selection, respectively, for events in class 2c. All distributions are obtained from 2000 data.

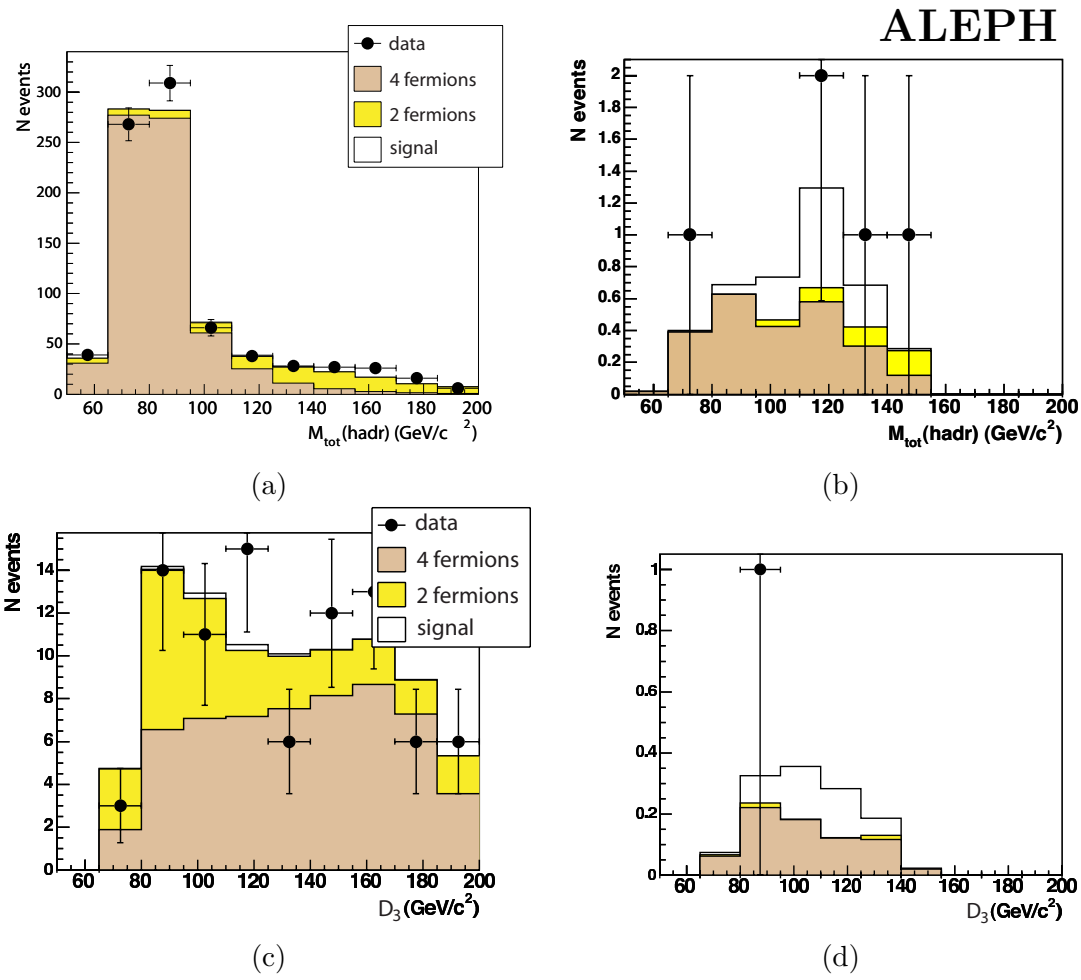

Figure 4: Discriminant variable, $M_{\mathrm{tot\ (hadr)}}$, for subclass 3a events after the preselection (a) and after the final selection cuts (b). Discriminant variable, D_3, for subclass 3b events after the preselection (c) and after the final selection cuts (d). All distributions are obtained from 2000 data.

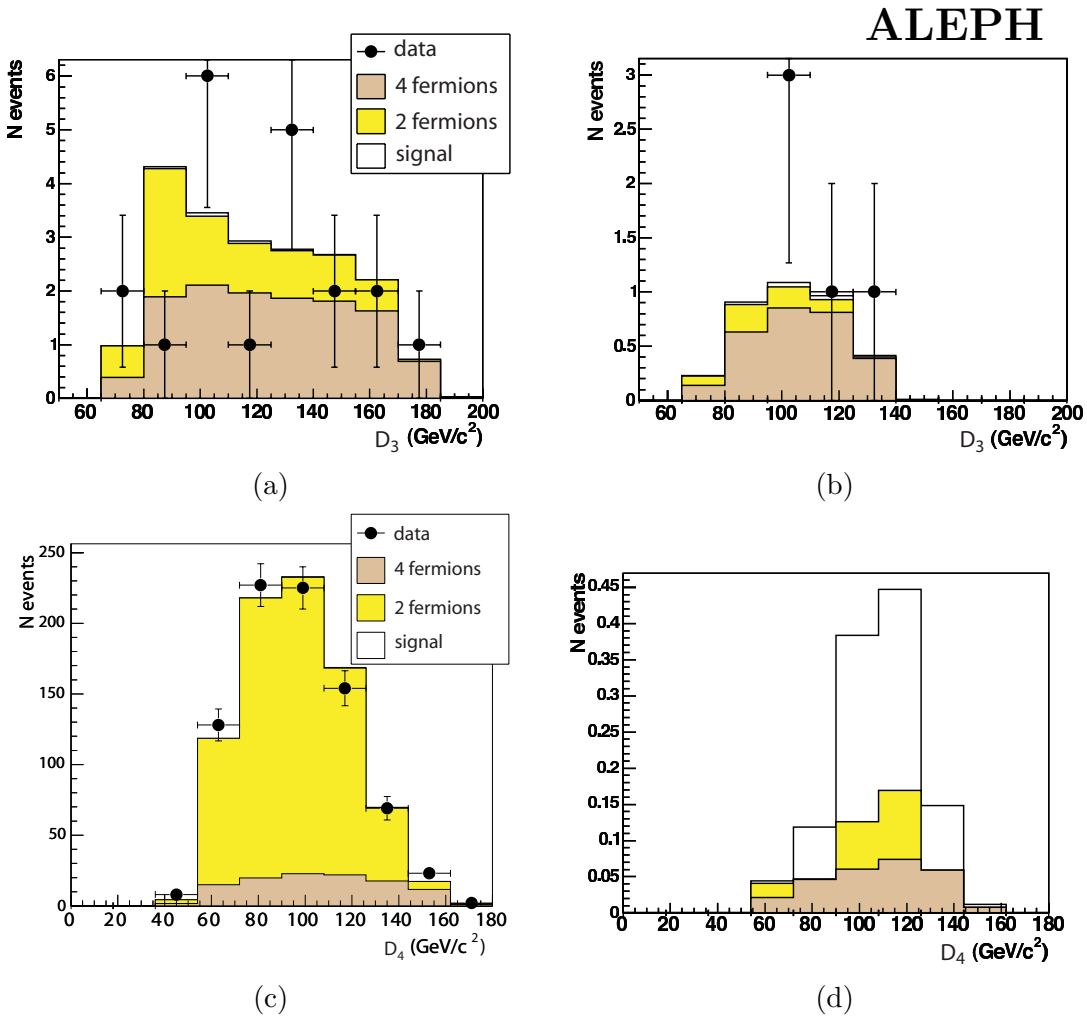

Figure 5: Discriminant variable, D_3, for subclass 3c events after the preselection (a) and the final selection (b). Discriminant variable, D_4, for subclass 3d events after the preselection (c) and the final selection (d). All distributions are obtained from 2000 data.

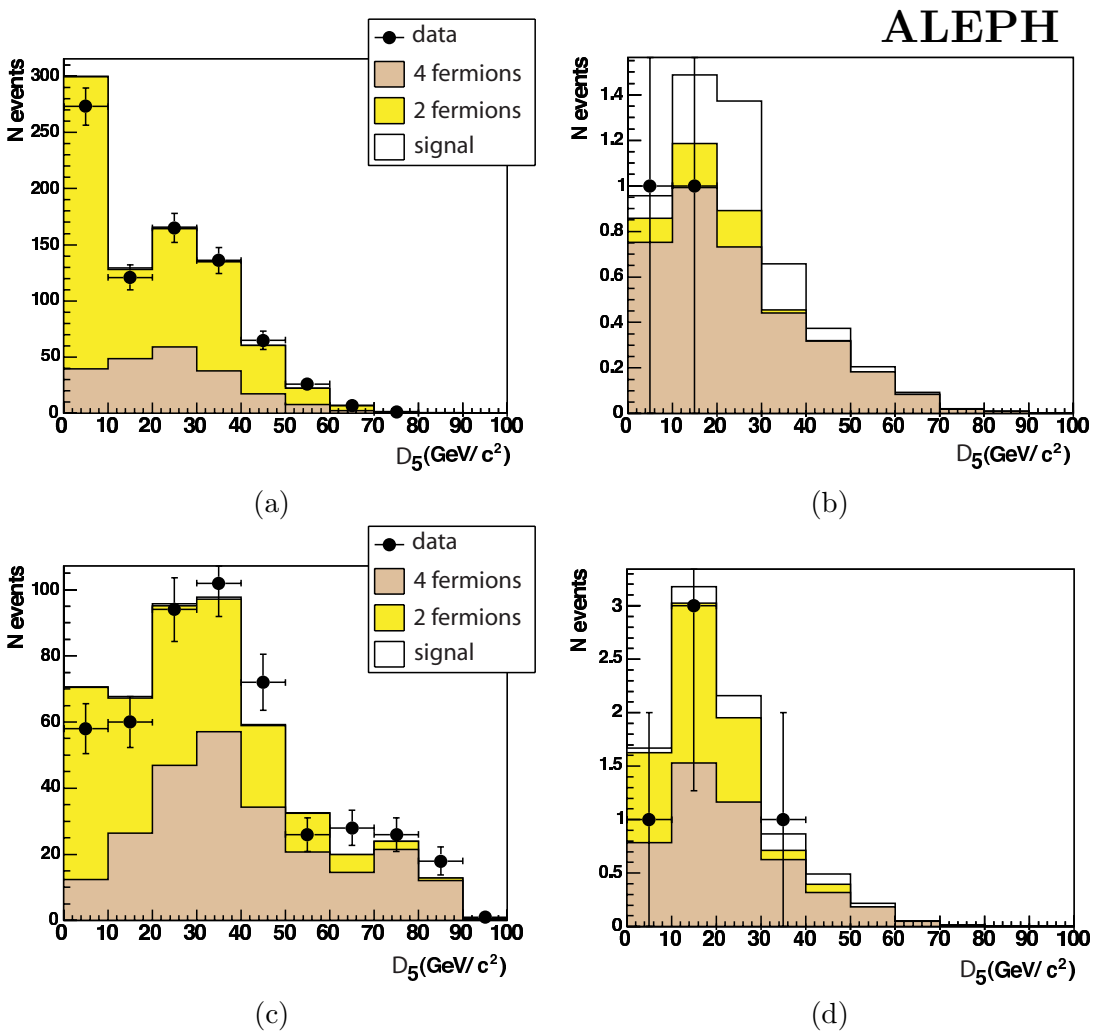

Figure 6: Discriminant variable for subclass 4a events after the preselection (a) and after the final selection cuts (b). Discriminant variable for subclass 4b events after the preselection (c) and after the final selection cuts (d). All distributions are obtained from 2000 data.

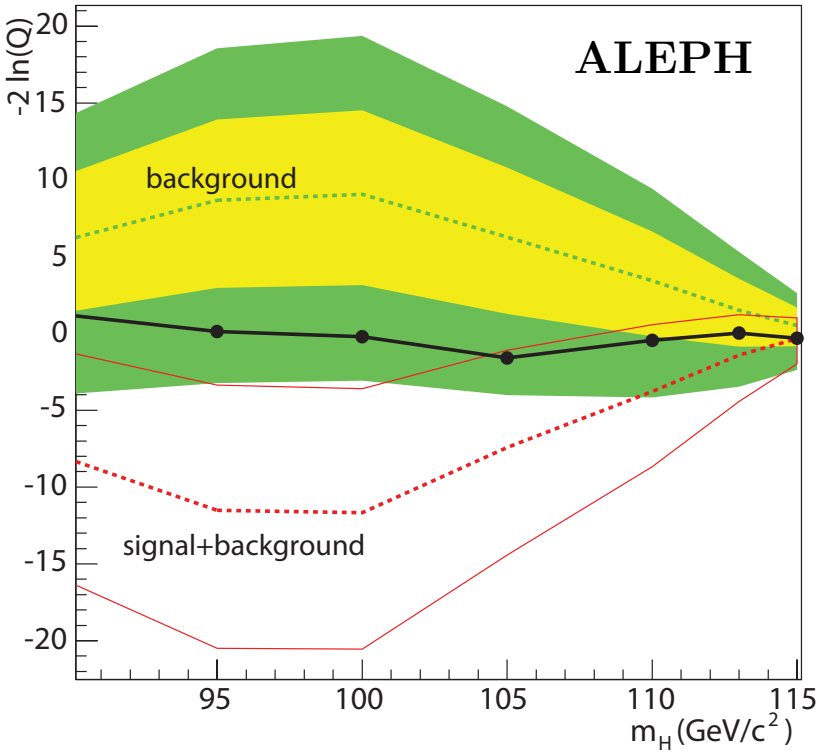

Figure 7: Log-likelihood ratio, $-2\ln Q$, as a function of the Higgs boson mass hypothesis, m_{H}, with all data collected between 191 GeV and 209 GeV. The solid line is the result obtained from the data. The expected background-only and signal-plus-background likelihoods are indicated by the dashed lines; the light and dark shaded bands around the background expectation contain 68% and 95% of the simulated background-only experiments, respectively. The 1σ bands for the signal-plus-background hypothesis are also shown.

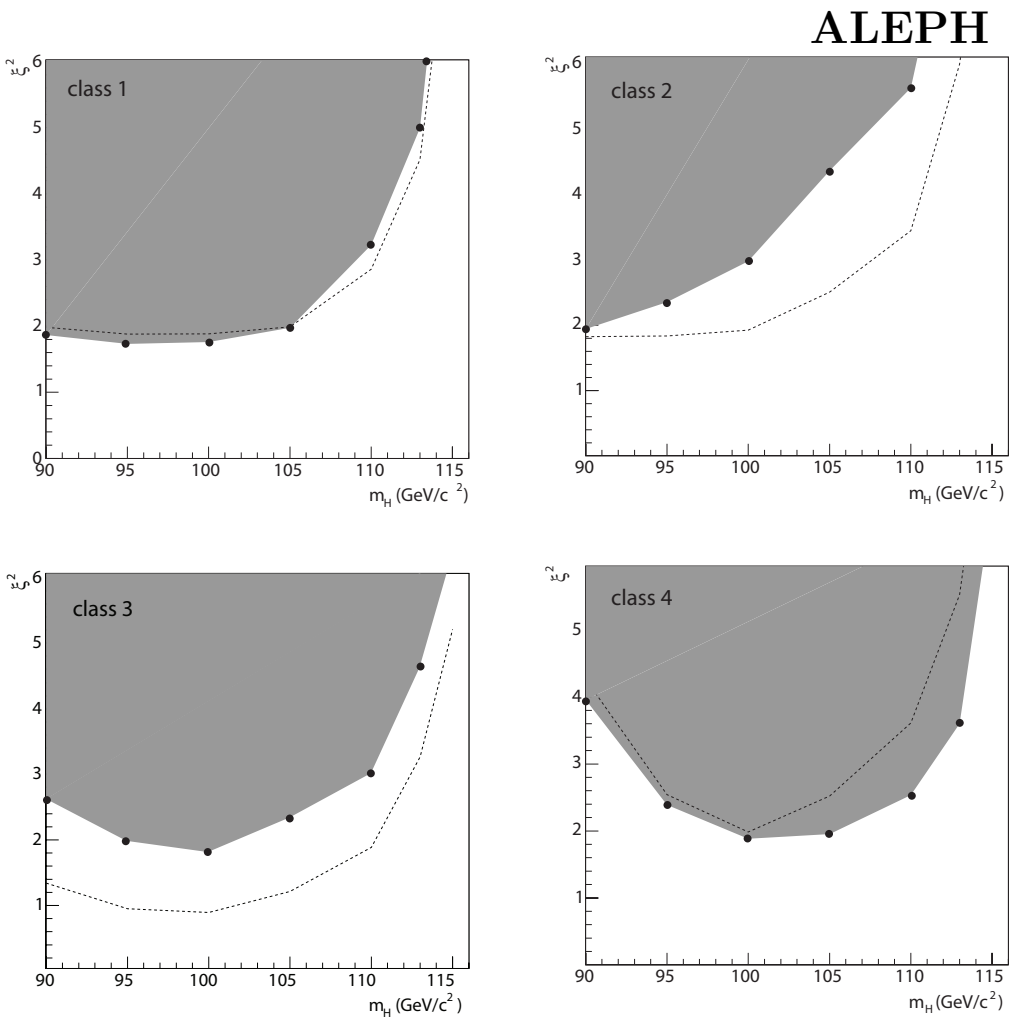

Figure 8: Limit on ξ^2 (defined in the text) as a function of the Higgs boson mass hypothesis, m_{H}, in the four different classes. The dashed line corresponds to the expected limit while the 95% C.L. excluded region is shown by the gray area.

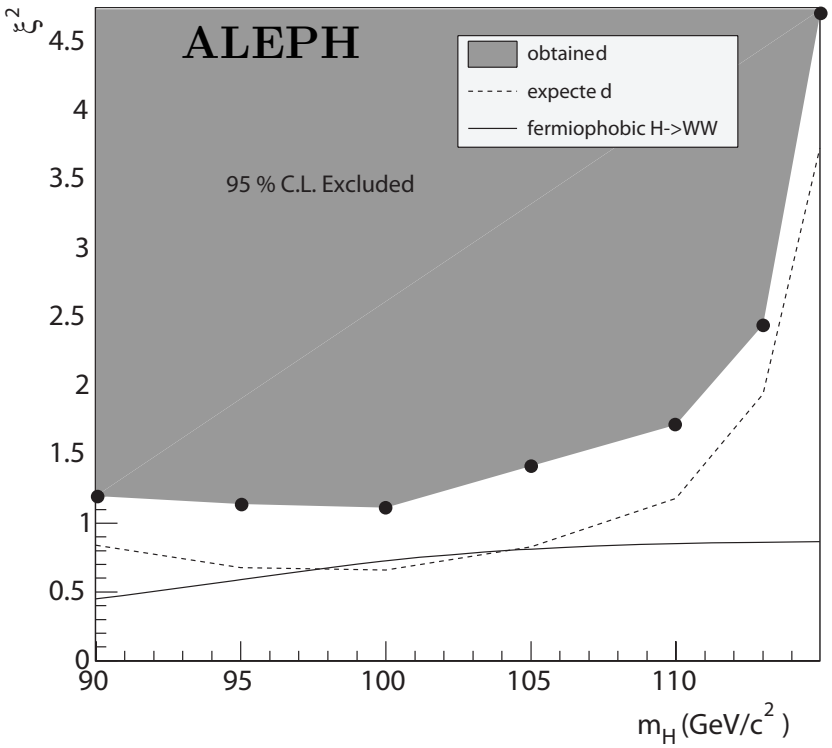

Figure 9: Limit on ξ^2 (defined in the text) as a function of the Higgs boson mass hypothesis, m_{H}. The dashed line corresponds to the expected limit while the 95% C.L. excluded region is shown by the gray area. The benchmark fermiophobic Higgs model branching ratio is depicted by the full line.

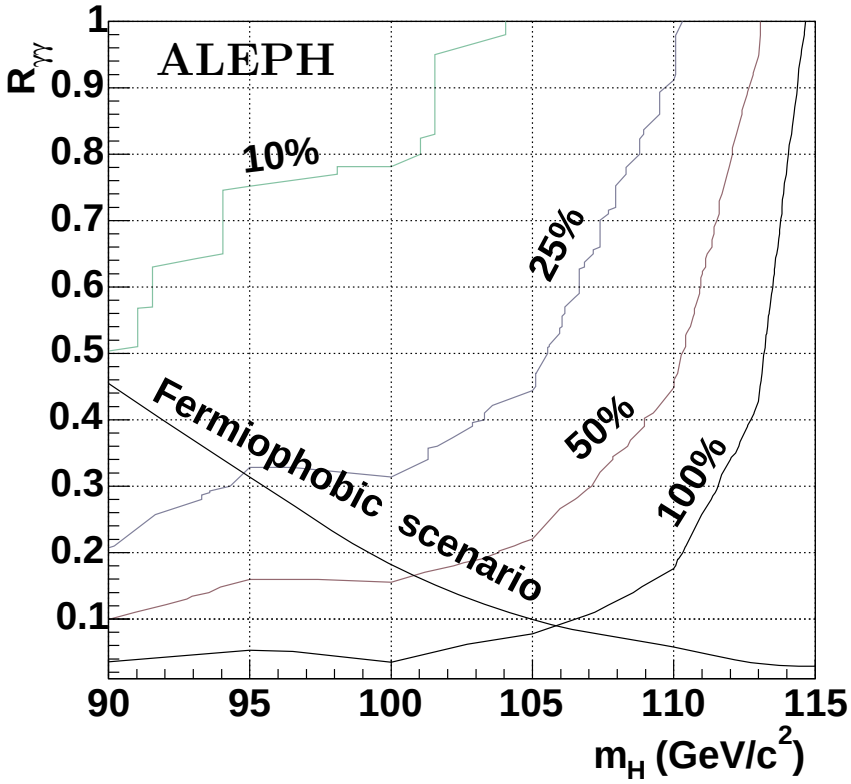

Figure 10: The 95% C.L. limit for $\mathrm{BR}_{\mathrm{bosons}}$ as a function of m_{H} and $\mathrm{R}_{\gamma\gamma}$. The solid lines indicate the upper limit of exclusion regions. The crossing point between the "$\mathrm{BR}_{\mathrm{bosons}} = 100\%$" line and the "Fermiophobic scenario" line provides the lower limit on the Higgs boson mass in the benchmark scenario: $m_{\mathrm{H}} > 105.8\,\mathrm{GeV}/c^2$.